First-principles investigations of atomic disorder effects on magnetic and structural instabilities in transition-metal alloys

M. Schröter*
Theoretische Tieftemperaturphysik, Gerhard-Mercator-Universität–Gesamthochschule Duisburg, Lotharstraße 1, 47048 Duisburg, Germany

H. Ebert†
Institut für Physikalische Chemie, Universität München, Theresienstraße 37-41, 80333 München, Germany

H. Akai‡
Department of Physics, Faculty of Science, Osaka University, 1-16 Machikaneyama, Toyonaka, Osaka 560, Japan

P. Entel,§ E. Hoffmann, and G. G. Reddy**
Theoretische Tieftemperaturphysik, Gerhard-Mercator-Universität–Gesamthochschule Duisburg, Lotharstraße 1, 47048 Duisburg, Germany
(Received 28 February 1995)

In this paper we use the coherent-potential approximation within the Korringa-Kohn-Rostocker band-structure scheme to investigate the influence of atomic disorder on magnetism and crystal structure of transition-metal alloys like iron-nickel. This method allows an investigation of disordered alloys on an equally well-defined basis as an investigation of corresponding stoichiometrically ordered phases. In particular we have calculated the magnetic and structural binding surfaces of fcc Fe_xNi_{1-x} for concentrations close to the critical concentration $x = 0.65$ which corresponds to the Invar alloy $Fe_{65}Ni_{35}$, with the help of the fixed-spin-moment method. We find that magnetism in the ground state gradually vanishes as we go from $Fe_{60}Ni_{40}$, which has a well-defined magnetic ground state being separated from the nonmagnetic state by 1.0 mRy/atom, to $Fe_{75}Ni_{25}$ which is nonmagnetic. The critical concentration for which this disorder driven magnetic-nonmagnetic transition occurs is $x \approx 0.65$–0.70 in accordance with the magnetic phase diagram of Fe_xNi_{1-x}. These calculations have to be compared with *ab initio* calculations for ordered fcc Fe_3Ni; here the magnetic ground state is by 1.25 mRy more stable than the nonmagnetic state. This different magnetic behavior of disordered and ordered phases can be explained on statistical grounds. Furthermore, the magnetic disordered ground state is unstable with respect to a martensitic fcc→bcc transition on the Fe-rich side in accordance with the structural phase diagram of Fe_xNi_{1-x}. We have furthermore calculated the temperature evolution of the binding surfaces with the help of a finite-temperature fluctuation theory. We find interesting reentrant ferromagnetic phase transitions in the fcc phase close to the Invar concentration $x = 0.65$.

I. INTRODUCTION

Recent first-principles calculations of the instability leading to the Invar effect (for recent reviews and further references see Refs. 1–5) have shown that the origin of the instability might be connected with a delicate balance of charge distribution between spin-polarized d orbitals of strongly antibonding and nonbonding character.[6] The associated thermal anomalies like small thermal expansion, softening of elastic constants with decreasing temperature, etc., may be explained on the basis of a phonon-assisted coherent transition of many electrons from strongly antibonding majority-spin states close to the Fermi energy E_F into empty minority-spin nonbonding orbitals just above E_F with increasing temperature. The associated rapid decrease of the magnetization can reduce the magnetic pressure as shown by partial pressure calculations.[7] This reduction of internal pressure could then compensate or even overcompensate the usual lattice driven thermal expansion resulting in a negative thermal expansion.[8]

In addition, the resonant coupling of the electrons to specific lattice modes like the shear TA_1 mode propagating in the fcc lattice in [110] and polarization in $[1\bar{1}0]$ direction, gives rise to a pseudogap at the Fermi level which is most pronounced in the minority-spin energy bands.[6] Our understanding is that this pseudogap is a many-particle effect arising from phonon-assisted mixing of spin-up and spin-down states at E_F. However, the tendency towards pseudogap formation is also seen in our one-electron band calculations for distorted lattices due to symmetry reduction. Such a pseudogap can actually pin part of the minority-spin bands relative to E_F. As a result the majority-spin bands would move upwards on the energy scale with increase in temperature until they coincide with the pinned minority-spin bands at the

Curie temperature T_c. Thus the lattice thermal expansion is partially hindered since the redistribution of some partial charges is also hindered due to the existence of this gap. This scenario holds as long as the system remains magnetic and the pseudogap exists.

Actually, there seems to be recent experimental evidence of this theoretically predicted pinning of minority bands in the magnetic state by spin-resolved photoemission from Fe-Ni and Invar alloys.[9] For Fe_xNi_{1-x} films with $x = 0.84$ and 0.5 the authors report pinning of the minority-spin-resolved intensity curve with respect to the Fermi energy independent of temperature, while the shape and position of the majority-spin-resolved intensity curve gradually approaches the Fermi energy. On the other hand, angle-resolved and spin-polarized photoemission studies on elemental Fe and Ni show that the exchange splitting of the electron distribution curves persists up and above T_c. This can be interpreted on the basis of the different temperature behavior of localized and itinerant contribution to the total magnetic moment. Since the intraband exchange energy is ~ 0.1 Ry per spin, the exchange splitting of the local part of the moment remains constant over the considered temperature range.[10] Therefore, the disappearance of the exchange splitting in Fe_xNi_{1-x} as observed by Kleemann *et al.*[9] is a remarkable effect showing that disorder can cause the exchange splitting to vanish on the time scale of photoemission studies as one approaches T_c.

While the investigations in Ref. 6 based on spin-polarized augmented-spherical-wave (ASW) band calculations within the local-density approximation (LDA) and atomic-sphere approximation (ASA) and the fixed-spin-moment (FSM) procedure, were done for stoichiometrically ordered Fe_3Ni, the real alloy Fe_xNi_{1-x} is disordered with random distribution of iron and nickel atoms on the fcc lattice. Since disorder as well as other defects can act as nucleation center for martensitic precursor effects and martensitc transitions, it is very important to know the influence of local environment effects caused by disorder[11] and its influence on the phase diagram of Fe_xNi_{1-x} which is shown in Fig. 1. Therefore, the aim of the present paper is a detailed discussion of the influence of disorder on the phase diagram for concentrations corresponding to the Invar composition and the formation of martensite.

The *ab initio* treatment of disorder with the ASW method is, apart from supercell calculations which are very time and memory consuming, not feasible. Therefore, we mainly have used the coherent-potential approximation within the Korringa-Kohn-Rostocker band-structure scheme based on the LDA (KKR-CPA LDA) which represents the most sophisticated method to treat the electronic structure of disordered alloys. A fast version of the KKR-CPA has recently been introduced by Akai[12] which also allows the evaluation of binding surfaces using the FSM method in reasonable computer time.

One should note, however, that we are not the first to apply the CPA method to ground-state and finite-temperature calculations of Fe-Ni alloys. In a series of papers Hasegawa and Kanamori have discussed the magnetic instability in Fe-Ni and related compounds.[13–15] In their first paper the electronic structure of Fe_xNi_{1-x} was obtained by using a nondegenerate tight-binding model and by employing the Hartree-Fock (HF) approximation together with the CPA. Model density of states for Fe and Ni and on-site energies ε_{Fe}, ε_{Ni}, correlation energies U_{Fe}, U_{Ni}, and electron numbers $n_{i\,Fe}$, $n_{i\,Ni}$ per site served as input, whereby ε_{Fe} and ε_{Ni} were fixed so that the Fermi energies of pure metals agree with each other in the nonmagnetic state leading to $\varepsilon_{Ni} < \varepsilon_{Fe}$. This energy difference now is very important since it leads to a considerable deformation of the minority-spin band, whereas the majority-spin band approximately keeps the original shape because the down-spin U term in the relation for the magnetic HF on-site energies

$$\begin{aligned}\varepsilon_{\uparrow Fe} - \varepsilon_{\uparrow Ni} &= \varepsilon_{Fe} - \varepsilon_{Ni} + (U_{Fe} n_{\downarrow Fe} - U_{Ni} n_{\downarrow Ni}) \\ &\ll \varepsilon_{\downarrow Fe} - \varepsilon_{\downarrow Ni} \\ &= \varepsilon_{Fe} - \varepsilon_{Ni} + (U_{Fe} n_{\uparrow Fe} - U_{Ni} n_{\uparrow Ni}) \qquad (1)\end{aligned}$$

cancels the difference of atomic energies while the up-spin U term vanishes for $x \to 1$ leaving $\varepsilon_{\downarrow Fe} - \varepsilon_{\downarrow Ni} = \varepsilon_{Fe} - \varepsilon_{Ni}$ for a wide range of x. For $x > 0.5$ the up-spin band passes the Fermi level leading to a rapid quenching of the Fe moment. This happens where the deviation of the magnetization from the Slater-Pauling curve starts. In subsequent papers the authors extended the CPA calculations to other systems and presented a revised calculation

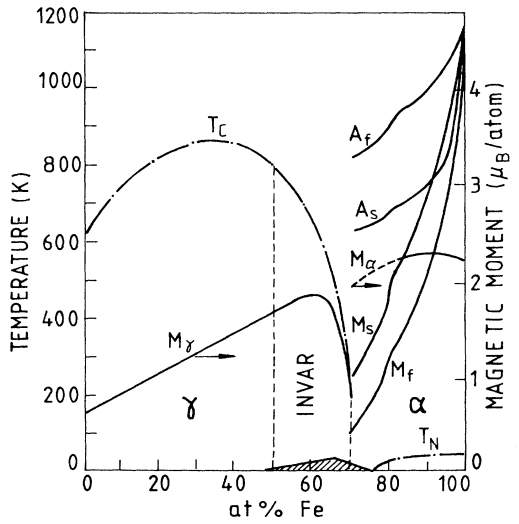

FIG. 1. Concentration dependence of Curie temperature T_c, magnetic moments M_γ (fcc), and M_α (bcc) of Fe_xNi_{1-x} (Refs. 85–88). The dashed region is a complicated mixed-magnetic phase with noncollinear spin arrangements (Ref. 89). Vertical dashed lines mark the Invar region and solid lines the austenite (A_s and A_f) transformation upon heating and the martensite (M_s and M_f) transformation upon cooling (the subscripts s and f refer to start and final). The separations between the M_s and M_f lines and the A_s and A_f lines are somewhat larger (Ref. 88) than earlier reported (Ref. 87). The phase diagram contains also the Néel temperature of the artificially stabilized γ phase on the iron-rich side (Ref. 37).

for Fe_xNi_{1-x}. Later work based essentially on the KKR-CPA method within the LDA has basically confirmed the findings of Hasegawa and Kanamori. The majority-spin density of states (DOS) is less deformed because the difference in the Fe and Ni Hartree potentials is canceled by the difference in the local exchange splittings (for example, see Ref. 12).

The present work can be considered as an extension of earlier works since, in addition, we have evaluated magnetic and structural binding surfaces showing how the ground state transforms upon alloying and thermal spin fluctuations at finite temperature. In contrast to Hasegawa and Kanamori our KKR-CPA results for the majority-spin DOS does not show a shift through E_F for concentrations $x < x_c \approx 0.70$. In our calculation the magnetic moment increases linearly with x and suddenly breaks down at the critical concentration x_c. This is in contradiction to the experimental observation (see Fig. 1) that the transition is rather moderate. This difference between experiment and theory was observed earlier[12,16,17] and can be attributed to the appearance of antiferromagnetic and spin-glass-like correlations which develop in the Invar region, while the KKR-CPA calculations have been performed only for ferromagnetic alignment of the spins.

In addition one should mention the first paper for finite-temperature calculations of Fe-Ni alloys with use of the CPA by Kakehashi.[18] Thermal expansion of Fe-Ni alloys was calculated on the basis of Liberman-Pettifor's virial theorem and the functional-integral method. In the calculation an effective two-band model (s and d) was used in order to investigate the influence of s-d charge transfer. Density of states and parameters were chosen so that the critical concentration of the ferromagnetic-paramagnetic transition occurs at $x_c = 0.65$. Results for the concentration and temperature dependence of the local magnetic moments and the specific heat show that anomalous thermal expansion in the Invar region is caused by large temperature variation of the Fe local magnetic moments due to single site excitations close to x_c. Kakehashi finds that in this region the specific heat term and the s-d charge transfer are not important. In addition to the KKR-CPA calculations, we have performed a supercell calculation for $x = 0.75$ which shows that a small amount of disorder leads to large fluctuations of the Fe local moments in the supercell. With increasing temperature this will allow for additional single-site excitations. This essentially confirms Kakehashi's picture. As discussed above, our more detailed electronic calculation shows that charge transfer close to the magneto-volume instability plays an important role. However, it is not the s-d charge transfer but the intra-atomic e_g-t_{2g} charge transfer which leads to a more rapid breakdown of the Fe moment with increasing temperature.

II. KORRINGA-KOHN-ROSTOCKER-COHERENT-POTENTIAL APPROXIMATION

A band-structure calculation based on the muffin-tin potential model (without LDA) together with the CPA was very early applied to the Fe-Ni system in order to obtain the residual resistivities for different concentrations.[19] The KKR-CPA (with LDA) has subsequently been developed.[20–23] It has turned out that this is a very powerful method to treat local environment effects in an *ab initio* manner. In this method the concept to treat disorder is rather simple while the underlying Hamiltonian is the same as that used in *ab inito* band-structure calculations; all the CPA does is to replace the random array of nonoverlapping muffin-tin potentials by an ordered array of effective potential wells whose scattering properties have then to be calculated self-consistently in the single-site CPA sense. This method was successfully applied to obtain total energy and pressure of nonmagnetic alloys like Cu_xZn_{1-x}.[24]

First *ab initio* calculations of the electronic structure of ferromagnetic disordered alloys like $Fe_{65}Ni_{35}$ based on local-spin-density treatment of exchange and correlation were presented by Johnson and Pinski.[25] The most striking result was as earlier observed by Hasegawa and Kanamori,[13–15] that electrons with different spin directions experience different degrees of disorder. The minority-spin electrons are more strongly influenced by disorder than the majority-spin electrons. Hence the minority-spin DOS is smooth in contrast to the very structured majority-spin DOS curve. In Fig. 2 we show for comparison the iron, nickel, and total DOS of ordered Fe_3Ni (Ref. 6) and of disordered $Fe_{75}Ni_{25}$ and $Fe_{60}Ni_{40}$ as obtained by KKR-CPA calculations. Apart from the position of the Fermi energy, the coarse-grained structures of the majority-spin DOS curves of Fe_3Ni and of $Fe_{75}Ni_{25}$ are very similar, whereas the smoothening effect of disorder is clearly visible in the minority-spin DOS curve. For the disordered $Fe_{75}Ni_{25}$ case we have used the experimental value for the lattice constant, $a = 6.833$ (a.u.), which yields a magnetic ground state with $M_{Fe} = 2.346\mu_B$ and $M_{Ni} = 0.644\mu_B$. This compares well with the extrapolated value for the γ moment in Fig. 1 at 75 at.% Fe. For the case of $Fe_{60}Ni_{40}$ the smoothening effect is even more serious. The main difference between the DOS curves of $Fe_{75}Ni_{25}$ and $Fe_{60}Ni_{40}$ is connected with a small shift of the minority-spin DOS to higher energies for $Fe_{75}Ni_{25}$, having the larger magnetic moment.

The fact that the minority states experience most of the disorder can also be discussed in the context of covalent magnetism.[26,27] The inset of Fig. 2(b) shows schematically the exchange splitting of the iron and nickel d states. The different effect of disorder is due to the different degree of hybridization between the majority-spin bands of Fe and Ni which are about equal in energy (because the difference in the Hartree potentials is cancelled by the difference in the exchange splittings), and the minority-spin bands of Fe and Ni which lie at different energies. What CPA essentially is doing, is to smear out this difference in the minority DOS by strongly mixing the Fe and Ni components.

As discussed in the introduction, the Invar effect can be related to the opening of a pseudogap at E_F. Therefore, it would be very important to repeat the calculations of Ref. 6 for the case of a distorted fcc lattice by using the KKR-CPA scheme, and to check whether the pseudogap in the minority-spin bands will be smeared out due to disorder or will survive. An inspection of Fig. 2(b)

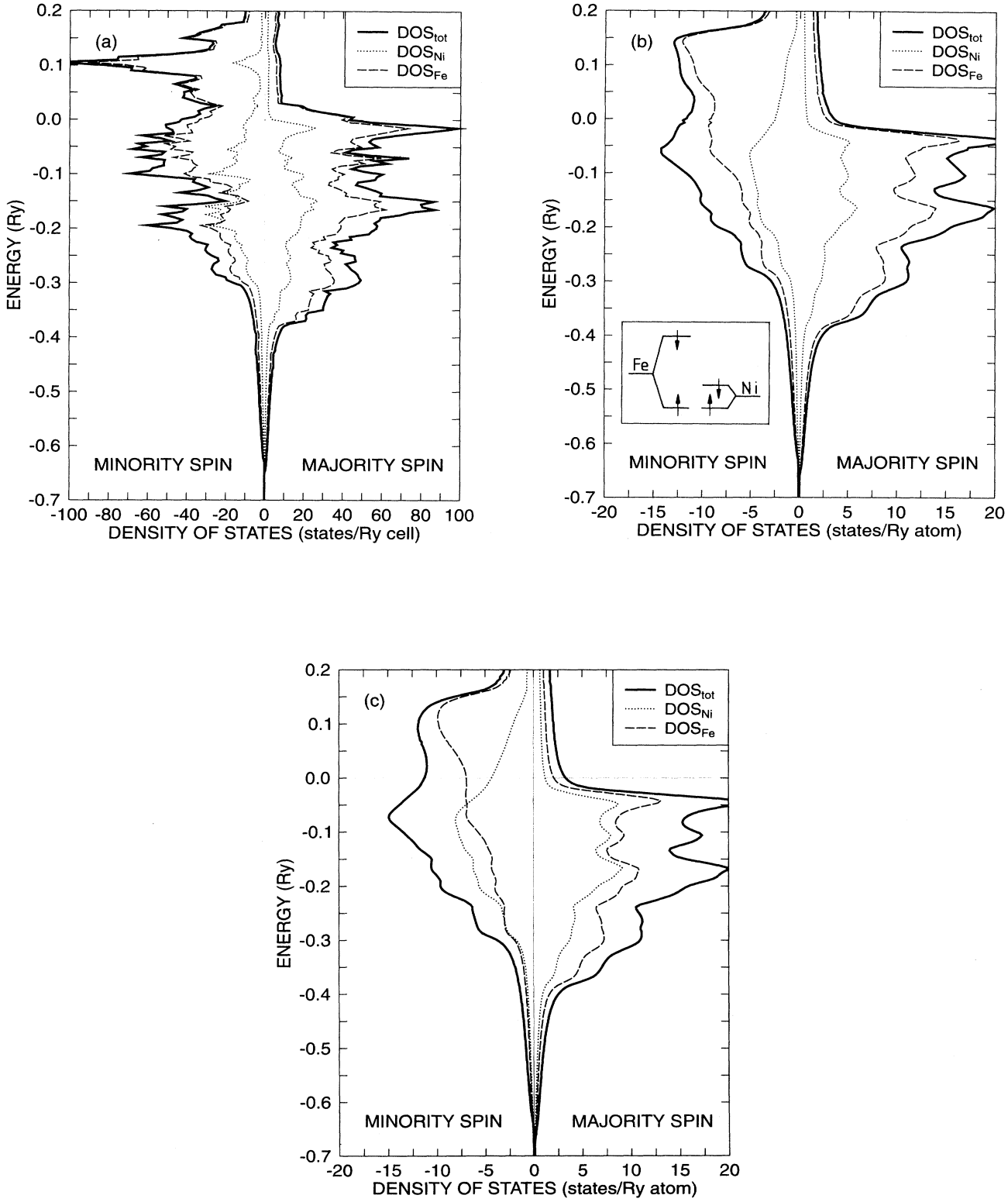

FIG. 2. Calculated majority and minority total and component densities of states of (a) ordered ferromagnetic Fe_3Ni, (Ref. 6), (b) of disorderd ferromagnetic $Fe_{75}Ni_{25}$ for the HM state at $a = 6.65$ (a.u.), and (c) of disordered ferromagnetic $Fe_{60}Ni_{40}$ (ground state) as obtained by KKR-CPA calcualtions. The DOS of $Fe_{65}Ni_{35}$ is nearly identical with (b). In (a) the DOS per unit cell is plotted in order to deploy curves. DOS per atom is obtained by dividing the Fe DOS by 3 and the total DOS by 4. The inset shows the difference between the energetic positions of the Fe and Ni majority and minority energy levels which explains why disorder effects mostly the minority DOS.

reveals that the Fermi level for $Fe_{65}Ni_{35}$ coincides with the nonbonding-antibonding valley of the minority-spin DOS. So it is likely that resonant minority-spin electron-phonon coupling can further deepen this valley.

In another paper the KKR-CPA scheme was applied to obtain the Slater-Pauling curves of fcc/bcc Fe_xNi_{1-x} and of bcc Fe_xV_{1-x},[28] which compare fairly well with experiment. Quite remarkably, also in bcc Fe_xV_{1-x} a pinning of the Fermi level in the bonding-antibonding valley of the minority-spin DOS was observed (being similar to the case of fcc $Fe_{65}Ni_{35}$) which seems to persist over a wide range of concentrations. In contrast, in the case of adding Ni to bcc Fe, this bonding-antibonding valley in the minority-spin DOS fills. Note that these properties can also be explained by the simplified scheme in Refs. 13–15.

This brief discussion of the KKR-CPA has shown that the influence of disorder in intermetallic alloys like Fe_xNi_{1-x} which can be perfectly mixed, is important and cannot be neglected. Altogether we have performed KKR-CPA calculations for 15 different Fe/Ni concentrations. Figure 3 shows the calculated phase diagram. The increase of the magnetization with increasing Fe concentration follows well the experimental observation apart from the first-order phase transition close to $x = 0.70$. The zero-temperature energy difference between the nonmagnetic and the ferromagnetic ground states simulates at least qualitatively the increase and decrease of the Curie temperature with increasing Fe concentration. Note that close in concentration to the magnetic moment collapse, energy differences for magnetic and structural transitions are of equal magnitude. For further discussion it would be enlightening to evaluate the effective parameters of exchange interactions by mapping the KKR-CPA results onto the Heisenberg model

$$\mathcal{H} = -\sum_{ij} J_{ij}\hat{\mathbf{S}}_i\hat{\mathbf{S}}_j, \tag{2}$$

where $\hat{\mathbf{S}}_i$ is the unit vector in the direction of the ith site magnetization, and where the exchange interaction can be related to the scattering path operator in the site (i,j) representation,[29,30] but at present we are unable to do this calculation. Approximately the Curie temperature would then be given by

$$k_B T_c \approx \frac{2}{3} J_0, \quad J_0 = \sum_{i \neq 0} J_{0i}. \tag{3}$$

This and similar procedures have sucessfully been applied to obtain the Curie temperatures of Fe and Ni (Refs. 30 and 31) and of Fe_3Pt.[32] In the following we discuss in detail the impact of atomic disorder on magnetism and the Invar effect.

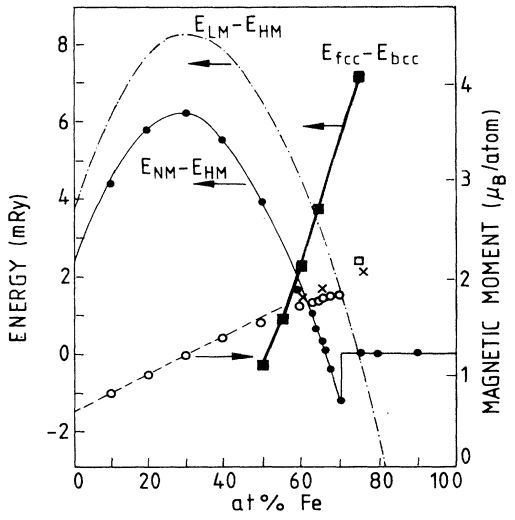

FIG. 3. Phase diagram of Fe_xNi_{1-x} as obtained from the KKR-CPA calculations. Open circles and crosses mark the magnetic moments in the γ and α phase, respectively. Filled circles mark the energy differences between the nonmagnetic and the HM ground states. For $x > 0.70$ filled circles have been placed at zero energy indicating that the HM state does no longer correspond to a local minimum on the binding surface. The curve through these points gives an impression of how the Curie temperature would behave. For comparison we show recent LMTO-CPA results obtained by Abrikosov *et al.* for the LM-HM energy difference (Ref. 90) (dashed dotted curve). These energy differences are similar to ours. Also marked are the KKR-CPA results for the energy differences between the fcc and the bcc states at different concentrations (filled squares). The open square is the result for Fe_3Ni. Note that he energy differences $E_{\mathrm{NM}} - E_{\mathrm{HM}}$ and $E_{\mathrm{fcc}} - E_{\mathrm{bcc}}$ are of comparable size at the onset of martensitic transformation.

III. MAGNETIC BINDING SURFACES OF Fe_xNi_{1-x}

We have calculated the magnetic binding surfaces, i.e., constant energy contour lines in the magnetization versus volume plane, for a set of specific concentrations corresponding to the Invar region of fcc Fe_xNi_{1-x} ($0.60 \leq x \leq 0.75$). The results are displayed in Figs. 4(a)–4(g).[33] The most striking result is that for the composition $Fe_{75}Ni_{25}$ the ground state of the disordered phase is already nonmagnetic and looks similar to the binding surface of pure fcc Fe,[34] whereas the *ab initio* calculation for the ordered phase yields a magnetic ground state which is displayed in Fig. 4(h). Note that Fe_3Ni there is only a small energy barrier of order 1.25 mRy or 197 K between the nonmagnetic (NM) local minimum and the stable high-moment (HM) solution at $\sim 1.5\mu_B$. For the disordered alloy the NM state is stable being separated from the HM state by ~ 3 mRy or 474 K. For the case of $Fe_{75}Ni_{25}$ we do not find a low-moment (LM) state corresponding to a local minimum on the binding surface in contrast to Fe_3Ni.[6]

The change of level sequence of HM and NM (LM) states with change in concentration x for the disordered case is shown in Fig. 5. Our calculations show that the Fe magnetic moment starts to become unstable at $x \approx 0.65 - 0.70$ which compares well with the experimental phase diagram shown in Fig. 1. As already noticed by Akai,[12] the phase transition from the ferromagnetic to the nonmagnetic state by following the $H = (\partial E/\partial M)_V = 0$ line, is of first-order which seems to

contradict experiment which shows a moderate variation of $M(T,x)$. However, the pressure experiments of Abd-Elmeguid and Micklitz[35] on fcc $Fe_{68.5}Ni_{31.5}$ and $Fe_{72}Pt_{28}$ show a rather rapid decrease of $T_c(p)$ for $p > 2$ GPa which means that both systems are close to a first-order magnetovolume instability. In fact, partial and total pressure calculations of ordered ferromagnetic Fe_3Ni show that the HM→LM transition is complete at a pressure of 6 GPa, completely in agreement with the experimental value for $Fe_{68.5}Ni_{31.5}$.[7] Approximately the same values for the pressure induced transition are obtained for the disordered case in Fig. 5, where the dashed lines show the pressure behavior for different concentrations. Note that the first-order transition has a very interesting concentration dependence. In the Invar region ($x \leq 0.65$) the first-order transion occurs at volumes lower than the HM ground state volume, whereas for $x > 0.65$ it occurs at volumes larger than the NM ground state volume. This may be called an Invar-Anti-Invar transition. In fact, alloys on the Fe-rich side ($x > 0.65$) with fcc structure

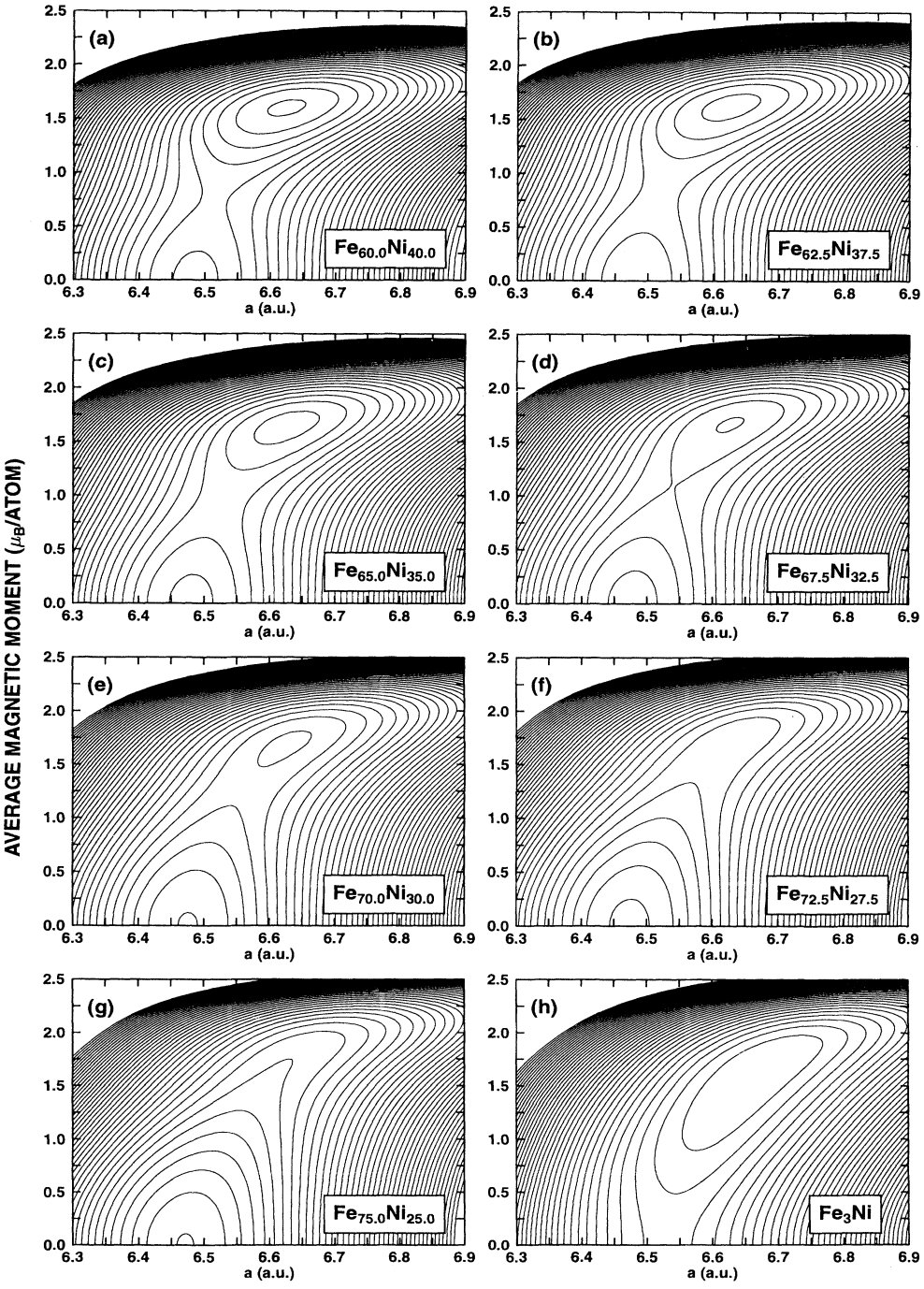

FIG. 4. Binding surfaces for the disorderd Fe_xNi_{1-x} system in the fcc structure in the concentration range $0.60 \leq x \leq 0.75$ as obtained by KKR-CPA calculations, (a)–(g). Contour lines are at 0.5 mRy intervals. True equilibrium corresponds to $H = (\partial E/\partial M)_V = 0$ and $p = -(\partial E/\partial V)_M = 0$. Upon changing x the system gradually transforms from (a) $Fe_{60}Ni_{40}$ being magnetic with energy minimum located at ($a = 6.625$ a.u., $M = 1.6\mu_B$/atom) to (g) $Fe_{75}Ni_{25}$ being nonmagnetic with energy minimum at ($a = 6.457$ a.u., $M = 0$). (h) shows the binding surface of orderd Fe_3Ni as obtained by ASW calculations with a stable magnetic ground state at ($a = 6.653$ a.u., $M = 1.5\mu_B$/atom).

behave as Anti-Invar systems. They have a nonmagnetic ground state and exhibit enhanced lattice expansion at high temperatures due to electronic excitations of in energy close lying HM states.[36]

It is interesting to consider the reasons why disordered $Fe_{75}Ni_{25}$ is nomagnetic in contrast to the ordered sample being magnetic. First, in the disordered case statistically some Fe atoms have nine or more nearest-neighbor Fe atoms in contrast to the eight nearest-neighbour (NN) Fe atoms for the ordered case (in fact, the binomial distribution function gives $\overline{n} = xN$ for the average number of NN Fe atoms out of $N = 12$ NN atoms being 9 for $x = 0.75$ and 7.8 for $x = 0.65$; see Fig. 6). Let us consider as a concrete example the interchange of two neighbored Fe and Ni atoms in ordered Fe_3Ni. The interchanged Fe atom has 11 (NN) Fe atoms which might destabilize its magnetic moment. Among these 11 NN atoms seven Fe atoms still have nine NN Fe atoms and four see eight NN Fe atoms but in a disordered array. Altogether this interchange effects approximately 32 atoms corresponding to eight neighboring unit cells ($Fe_{24}Ni_8$). This cluster may have at its origin a nonmagnetic Fe atom or an Fe atom with a reversed spin, and Fe atoms with low moments in its neighborhood. Interchange of more Fe-Ni atoms will lead to interacting clusters which finally destabilize the magnetic state. Therefore, the disordered case is a system being closer to pure fcc Fe which has a nonmagnetic ground state[37] (the HM ferromagnetic fcc Fe phase cannot exist since it is unstable with respect to the shear deformation; the energy difference $E_{\mathrm{NM-fcc}} - E_{\mathrm{FM-bcc}}$ is of the order of 5.31 mRy/atom[38]). We have checked this assumption by performing an ASW-ASA supercell calculation for simple tetragonal $Fe_{24}Ni_8$ for the case that the central Ni atom and one neighboring Fe atom have been interchanged. This leads to a unit cell with 16 inequivalent atoms with magnetic moments listed in Table I. The most striking result is that the interchanged Fe atom has now a reversed magnetic moment of $-1.91\mu_B$ and that the perturbation is long ranged as can be seen in Fig. 7; i.e., we find alternating Fe-Ni and Fe-Fe layers with considerably reduced and less reduced Fe magnetic moments, respectively. Of course, one would have to perform larger supercell calculations with different kinds of simulated disorder but this is beyond our computer capacities. But starting from this zero-temperature scenario, it is tempting to assume that finite temperatures will give rise to large amount of excitations of the local Fe moments. This comes close to Kakehashi's result that single site excitations of the Fe moments dominate in the Invar region.[18] Unfortunately this kind of behavior of the Fe moments is not contained in the KKR-CPA calculations which assume parallel alignment of all magnetic moments.

This supercell scenario agrees with the interpretation of Mössbauer investigation of Invar from which follows

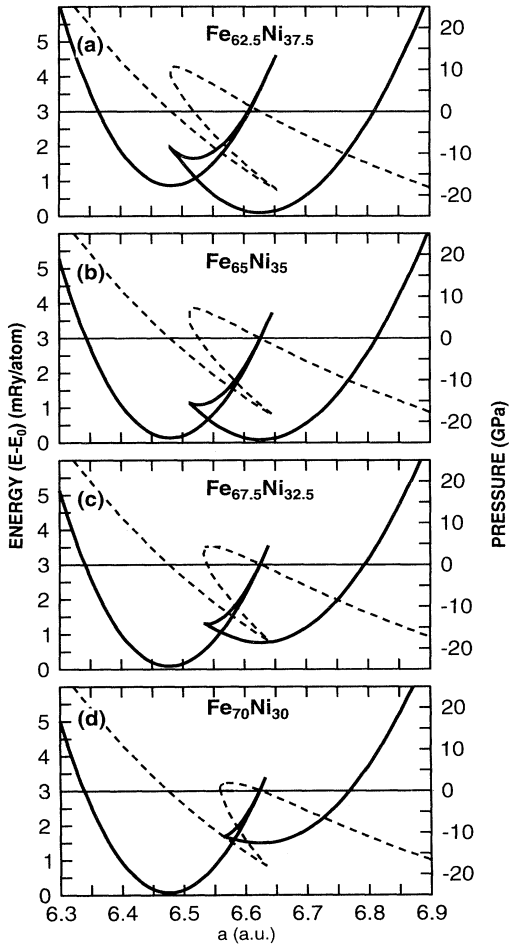

FIG. 5. Change of level sequence of HM and NM states with change in concentration in Fe_xNi_{1-x}. Here the energy relative to the ground-state energy is plotted as function of the lattice constant along the $H = (\partial E/\partial M)_V = 0$ line for each concentration. All data points are plotted on the same scale. The third minimum in between the NM state (left minimum) and the HM state (right minimum) does not correspond to a local minimum on the binding surface but to the saddle point, where the $H = P = 0$ lines cross. Also shown is the pressure dependence (dashed line). Horizontal line marks the zero-pressure line. The first-order transition is in the Invar region ($x \leq 0.65$) at volumes lower than the ground-state volume and moves to larger volumes for $x > 0.65$ which corresponds to an Invar-Anti-Invar transition (Ref. 36). Anti-Invar behavior is typical of enhanced paramagnets (Ref. 91).

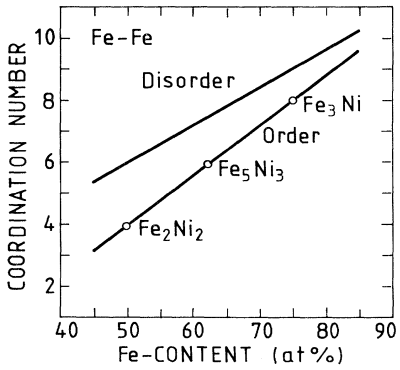

FIG. 6. Coordination numbers of Fe atoms around an Fe atom in ordered and disordered phases with fcc structure as a function of Fe content.

that the Fe magnetic moment becomes unstable for less than three NN neighbor Ni atoms.[39] Another point is that since the disordered system behaves statistically as if fewer Ni atoms were present we have, on the average, less carriers in the strongly antibonding Ni bands which causes the volume to shrink and the magnetization to become smaller. Furthermore this brings E_F closer to the antibonding peak in the majority-spin DOS of mainly t_{2g} character, which can further destabilize the Fe magnetic moment.[40]

A more general discussion of clustering processes in Fe_xNi_{1-x} is difficult since metallic nature and itinerant magnetism seem to mask many purely statistical features of a system containing two types of atoms. For example, the percolation process leads to the following result for the mean cluster size in random site mixtures on the fcc lattice:[41]

$$S(x) \simeq C(x_c - x)^{-\gamma}, \quad x \to x_c^- \tag{4}$$

with

$$x_c = 0.198 \pm 0.003, \quad \gamma = 1.66 \pm 0.07, \quad C = 0.101 \pm 0.001 \quad \text{(fcc lattice)}, \tag{5}$$

$$x_c = 0.245 \pm 0.004, \quad \gamma = 1.66 \pm 0.07, \quad C = 0.142 \pm 0.001 \quad \text{(bcc lattice)}. \tag{6}$$

TABLE I. Supercell-ASW results of local magnetic moments in $Fe_{24}Ni_8$ for the case that the central Ni atom at position $(\frac{1}{2}, \frac{1}{2}, \frac{1}{2})$ and neighboring Fe atom at $(\frac{1}{4}, \frac{1}{4}, \frac{1}{2})$ have been interchanged.

Atom	Atomic position	Magnetic moment (μ_B)
1 (Ni)	$(0,0,0)$	0.4219
2 (Fe)	$(\frac{1}{4}, \frac{1}{4}, 0)$	1.9399
3 (Fe)	$(\frac{1}{4}, 0, \frac{1}{4})$	2.1554
4 (Fe)	$(0, \frac{1}{4}, \frac{1}{4})$	2.1554
5 (Fe)	$(\frac{1}{4}, 0, \frac{3}{4})$	2.1554
6 (Fe)	$(0, \frac{1}{4}, \frac{1}{4})$	2.1554
7 (Ni)	$(0, 0, \frac{1}{2})$	0.4489
8 (Ni)	$(\frac{1}{4}, \frac{1}{4}, \frac{1}{2})$	0.4578
9 (Ni)	$(0, \frac{1}{2}, 0)$	0.4317
10 (Ni)	$(\frac{1}{2}, 0, 0)$	0.4317
11 (Fe)	$(\frac{1}{4}, \frac{3}{4}, 0)$	1.2990
12 (Fe)	$(\frac{3}{4}, \frac{1}{4}, 0)$	1.2990
13 (Fe)	$(\frac{1}{4}, \frac{1}{2}, \frac{1}{4})$	1.8843
14 (Fe)	$(\frac{1}{4}, \frac{1}{2}, \frac{3}{4})$	1.8843
15 (Fe)	$(\frac{1}{2}, \frac{1}{4}, \frac{1}{4})$	1.8843
16 (Fe)	$(\frac{1}{2}, \frac{1}{4}, \frac{3}{4})$	1.8843
17 (Fe)	$(0, \frac{3}{4}, \frac{1}{4})$	2.0098
18 (Fe)	$(0, \frac{3}{4}, \frac{3}{4})$	2.0098
19 (Fe)	$(\frac{3}{4}, 0, \frac{1}{4})$	2.0098
20 (Fe)	$(\frac{3}{4}, 0, \frac{3}{4})$	2.0098
21 (Ni)	$(0, \frac{1}{2}, \frac{1}{2})$	0.4771
22 (Ni)	$(\frac{1}{2}, 0, \frac{1}{2})$	0.4771
23 (Fe)	$(\frac{1}{4}, \frac{3}{4}, \frac{1}{2})$	1.0238
24 (Fe)	$(\frac{1}{2}, \frac{1}{4}, \frac{3}{4})$	1.0238
25 (Ni)	$(\frac{1}{2}, \frac{1}{2}, 0)$	0.3585
26 (Fe)	$(\frac{3}{2}, \frac{3}{4}, 0)$	1.7502
27 (Fe)	$(\frac{3}{4}, \frac{1}{2}, \frac{1}{4})$	1.7151
28 (Fe)	$(\frac{1}{2}, \frac{3}{4}, \frac{1}{4})$	1.7151
29 (Fe)	$(\frac{3}{4}, \frac{1}{2}, \frac{3}{4})$	1.7151
30 (Fe)	$(\frac{1}{2}, \frac{3}{4}, \frac{3}{4})$	1.7151
31 (Fe)	$(\frac{1}{2}, \frac{1}{2}, \frac{1}{2})$	−1.9128
32 (Fe)	$(\frac{3}{4}, \frac{3}{4}, \frac{1}{2})$	1.6126

An inspection of Fig. 1 or of the experimental data for magnetization, specific heat, resistivity, etc., does not show any anomalous behavior of physical observables at or close to the critical Fe concentration on the Ni-rich side. Nor does the KKR-CPA calculation give any anomalous results for concentrations close to $x = 0.198$ at. % Fe where the Fe cluster percolates. It seems as if one mixes two perfectly soluble systems, where the physics is determined by the intinerant nature of the electrons. On the other hand, the other critical concentration on the Fe-rich side is that for the percolating Ni cluster, $1 - x = 0.198$, being close to the concentration $x \approx 0.3$ for which magnetism disappears in disordered Fe_xNi_{1-x}. Perhaps it is not too speculative to conclude that for Ni concentrations for which the biggest Ni cluster is no

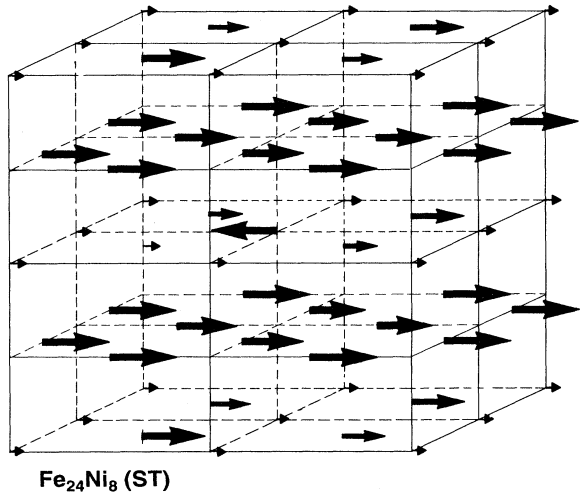

FIG. 7. ASW results for the distribution of magnetic moments in $Fe_{24}Ni_8$ for the case that the central Ni atom and one neighboring Fe atom have been interchanged. Length of the arrows are relative to the arrow of the central Fe atom which has a reversed magnetic moment of $-1.91\mu_B$. The resulting decrease of the average magnetic moment per atom is from $1.51\mu_B$ for stoichiometric order to $1.33\mu_B$ corresponding to a 11.25% reduction (compare also Table I).

longer percolative, also magnetism vanishes in the fcc lattice. Furthermore, there is some structure in the austenite and martensite transformation temperatures in Fig. 1 close to the concentration where Ni percolates. Whether this is coincidence or physics is unclear at present.

It is now very tempting to imagine that for a given nominal concentration, for example $x = 0.65$, one might find in the real disordered alloy in different regions of the sample the different energy conditions $E(a, M)$ shown in Figs. 4(a)–4(h) due to local fluctuations of the concentration leading to alternating regions of local HM, LM, and NM states. Such a distribution of many different HM and LM states in real space (together with noncollinear alignment between moments of Fe-rich and Ni-rich regions) can explain the unusual saturation magnetization $M(T)$ curves of various fcc Fe-Ni alloys close to the composition $Fe_{65}Ni_{35}$ which lie much below the usual mean-field curve in contrast to ordinary ferromagnets (see Fig. 30 in Ref. 3). Also the difference between the Invar alloys Fe-Ni and Fe-Pt can be explained on the same basis. For the composition $Fe_{72}Pt_{28}$ both, the disordered as well as the ordered sample are magnetic in contrast to $Fe_{75}Ni_{25}$. The magnetic state in Fe-Pt is more easily stabilized for ordered and disordered phases because the rather large atomic volume of the Pt atom guarantees that the ground state is the high-volume HM state. For further theoretical discussion of the differences between Fe-Ni and Fe-Pt Invar alloys see Refs. 42 and 43.

The concentration dependence of equilibrium lattice constant, local moments at Fe and Ni sites and the magnetization, hyperfine fields, and the Fe isomer shift has already been discussed in Ref. 12 for the Fe-rich side of Fe_xNi_{1-x} and will not be repeated here. Altogether one may say that the results agree fairly well with experiment.

Finally one should say that the scenario displayed in Figs. 4(a)–4(h) is not identical to that of the Weiss model which originally was introduced as a two-states model to account for the possibility of HM→LM transition as an internal electronic excitation in fcc Fe-Ni with increasing temperature.[44] We think that our results differ greatly from Weiss. The Weiss model concentrates on individual Fe atoms. In effect, it says there are two different kinds of Fe in Invar — a high-spin–high-volume and a low-spin–low-volume variety. Accepting it, one would be forced to think of a mixed-valence system. Our present day lingo considers the state of the (entire) system — or the state of local clusters. Therefore, we do not expect that a local-moment theory would be a good starting point for the discussion of the Invar effect in spite of its success in fitting experimental data.[45]

Despite the fact that disordered $Fe_{75}Ni_{25}$ is nonmagnetic while the ordered compound is magnetic, one may still use the latter as an Invar model for pedagogical reasons.[46–50,55,56] Also, discussion of band structures obtained for the ordered alloy is somewhat easier than a detailed analysis of the spectral function for the disordered case which is defined by

$$A(\mathbf{k}, E) = \frac{1}{\pi}\mathrm{Im}\,\frac{dZ(\mathbf{k}, E)}{dE}, \tag{7}$$

where

$$\begin{aligned} Z(\mathbf{k}, E) = &\ln\det\left[(\mathbf{k}+\mathbf{g})^2 - E\right] \\ &+ \ln\det\left[t^{-1}(E) - G_0(\mathbf{k}, E)\right] \\ &+ x_A \ln\det\left\{1 + \tau(E)\left[t_A^{-1}(E) - t^{-1}(E)\right]\right\} \\ &+ x_B \ln\det\left\{1 + \tau(E)\left[t_B^{-1}(E) - t^{-1}(E)\right]\right\} \end{aligned} \tag{8}$$

is a measure of the total number of states below the (real) energy E. G_0 is the structural Green's function of the KKR band-structure method connected with the scattering path operator $\tau(E)$ and CPA t-matrix which has to be determined self-consistently, by

$$\tau(E) = \frac{1}{\Omega_{\mathrm{BZ}}}\int_{\mathrm{BZ}} d^3k\ \left[t^{-1}(E) - G_0(\mathbf{k}, E)\right]^{-1}, \tag{9}$$

$$\begin{aligned} \tau(E) = &\ x_A\left[t_A^{-1}(E) - t^{-1}(E) + \tau^{-1}(E)\right]^{-1} \\ &+ x_B\left[t_B^{-1}(E) - t^{-1}(E) + \tau^{-1}(E)\right]^{-1}. \end{aligned} \tag{10}$$

Here x_A (x_B) and t_A (t_B) are the concentration and the t matrix of the muffin-tin potential of the A (B) atom, respectively.[12]

We have evaluated the spectral function corresponding to the momentum and energy resolved DOS (*band structure*) for the alloy $Fe_{75}Ni_{25}$ along the main symmetry directions of the fcc lattice Brillouin zone (BZ). Results for the HM and NM states [see Fig. 4(g) at $a = 6.65$ or $r_{\mathrm{WS}} = 2.60$ and at $a = 6.47$ or $r_{\mathrm{WS}} = 2.53$, respectively] are shown in Figs. 8(a)–8(c). A rather big imaginary part of 3 mRy has been attached to the real energies in order to smooth those parts of the spectrum which have remained δ-function-like. Summation over momentum then leads to the DOS in Fig. 2(b). It is obvious from the figures that the KKR-CPA band structure resembles hybridizing (s, p) and e_g- and t_{2g}-like d bands.

In order to see the difference between disordered and ordered cases, we have made a similar calculation for Fe_3Ni by plotting the imaginary part of the Dyson equation

$$\mathcal{G}_{n\sigma}(\mathbf{k}, z) = \frac{1}{z - \varepsilon_{n\sigma}(\mathbf{k}) - \Sigma_{n\sigma}(\mathbf{k}, z)} \tag{11}$$

for each band n and spin polarization σ (not in the fcc but in the sc Brillouin zone). Here $\varepsilon_{n\sigma}(\mathbf{k})$ are the Bloch energies calculated with the ASW-ASA method; $\Sigma_{n\sigma}(\mathbf{k}, z)$ is the self-energy which can be assumed to arise from zero-temperature quantum fluctuations. The momentum and energy-resolved DOS is then given by

$$A_{n\sigma}(\mathbf{k}, E) = -\frac{1}{\pi}\mathrm{Im}\,\mathcal{G}_{n\sigma}(\mathbf{k}, E), \tag{12}$$

where for simplicity the self-energy has been chosen to be 12 mRy for each momentum and energy. The result is shown in Fig. 9 for the up- and down-spin case. In spite of four times more bands as compared to the KKR-CPA case, the momentum integrated curves lead to the result in Fig. 2(a) which, apart from the fine structure, resembles the KKR-CPA DOS in Fig. 2(b). This shows that for some integrated electronic quantities the difference between the disordered and ordered cases can be rather small.

In order to get further insight, it would be nice if

these first-principles calculations could be pursued at finite temperatures. This is beyond present day computer capabilities (in spite of first attempts do this, for example, by using the disordered local-moment picture,[57] or by introducing effective-spin Hamiltonians[58]). However, the zero-temperature results presented in this section can be used as input into a finite-temperature fluctuation theory which allows the evaluation of the temperature dependence of thermal expansion, bulk modulus, heat capacity, magnetization, pressure dependence of T_c, high-field susceptibility, etc.[51–56] This is discussed in the next section.

IV. FINITE-TEMPERATURE FLUCTUATION THEORY

The finite-temperature fluctuation theory allows us to extend the discussion of results obtained in zero-temperature *ab initio* calculations to finite temperatures.[6,51–56,59] The basic ingredients are magnetization and volume, both taken as thermodynamic variables which are allowed to fluctuate around their mean values at finite temperatures. The functional used for the energy is the following:

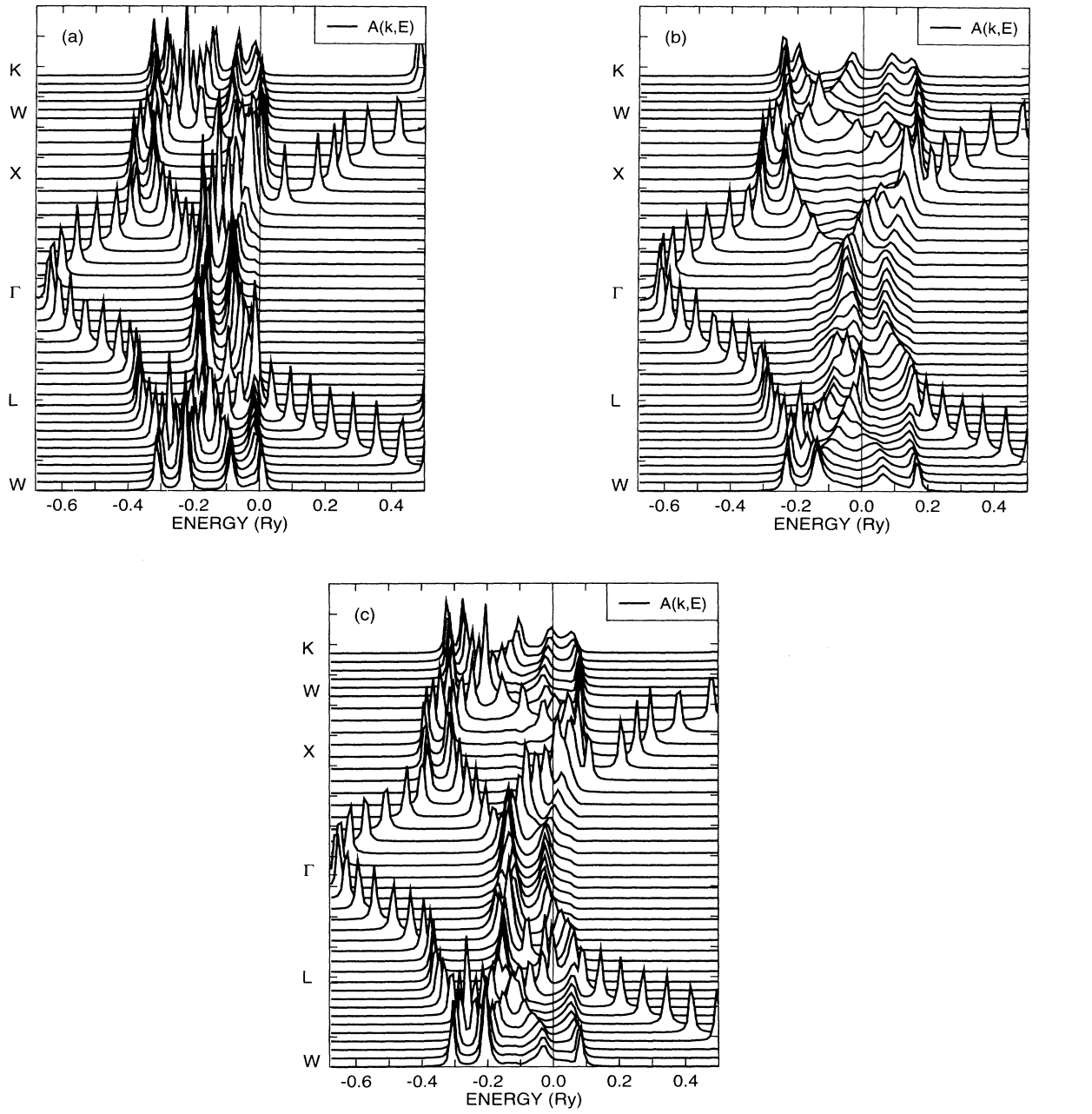

FIG. 8. (a) Majority-spin and (b) minority-spin KKR-CPA bands of $Fe_{75}Ni_{25}$ in the HM state at $a = 6.65$ (a.u.); (c) nonmagnetic KKR-CPA bands of $Fe_{75}Ni_{25}$ for $a = 6.47$ (a.u.).

$$\mathcal{H}[\mathbf{m},\omega] = \frac{1}{V}\int_V d^3r \left(g_m \sum_{\alpha,\beta} (\nabla_\alpha \mathbf{m}_\beta)^2 + a(\omega_c - \omega)\mathbf{m}^2 + a'\omega^2\mathbf{m}^2 + b\,\mathbf{m}^4 + c\,\mathbf{m}^6 + g_\omega(\nabla\omega)^2 + \frac{\kappa}{2}\omega^2 + \gamma\,\omega^3 + \delta\,\omega^4 \right). \tag{13}$$

The thermodynamic variables are split into static and fluctuating parts,

$$\mathbf{m}(\mathbf{r},T) = \mathbf{m}_0(T) + \mathbf{m}'(\mathbf{r},T), \tag{14}$$

$$\omega(\mathbf{r},T) = \omega_0(T) + \omega'(\mathbf{r},T), \tag{15}$$

where

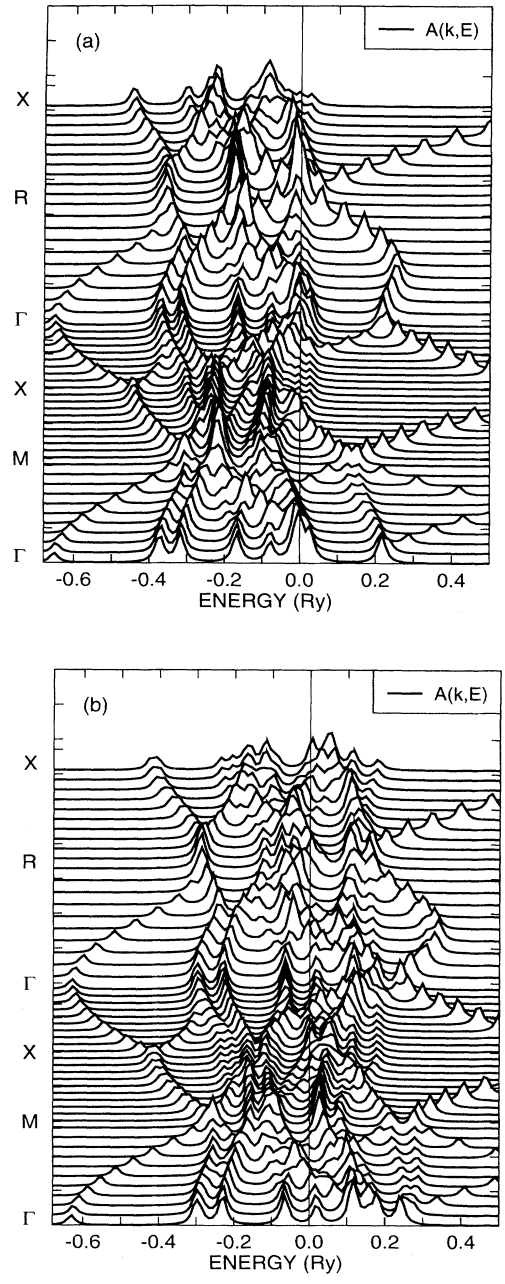

FIG. 9. Momentum and energy resolved DOS (*bands*) of (a) majority and (b) minority spins of Fe_3Ni.

$$\omega(T) = \frac{a^3(T) - a_0^3}{a_0^3} \tag{16}$$

is taken as the appropriate volume variable with the nonmagnetic ground-state lattice constant $a_0 = 6.48$ a.u. as reference for the case of Fe_xNi_{1-x}.

We would like to point out that the finite-temperature spin- and volume-fluctuation theory based on this Landau-type effective Hamiltonian is suitable for the description of weak magnetism in which long-wave thermal spin fluctuations are dominant, while Fe-Ni alloys can be characterized by the anomalies in the intermediate interaction strength between strong and weak magnets. Therefore, we have paid particular attention when calculating the Landau coefficients from a least-mean-square fit to the *ab initio* band-structure results. All series obtained so far showed fairly good convergence properties. Of course this still does not allow for a good description of strong magnets in the Landau-Ginzburg frame (further drawbacks of the fluctuation theory were already critically discussed in Ref. 54). But some results give at least an impression of what might happen at finite temperatures. The calculated mean-square fluctuation amplitudes differ in magnitude not too much from results in Refs. 60 and 61 obtained for Fe and Ni with the Hubbard model and the functional-integral method.[62] We think also that the behavior of the finite-temperature binding surfaces gives at least an impression of how spin and volume fluctuations destroy the HM state.

Important for the discussion of the influence of fluctuations is the *equal-time correlation function* at temperatures above T_c which is easily obtained from the finite-temperature fluctuation theory giving

$$\langle \mathbf{m}^2(\mathbf{k}) \rangle_0 = \frac{3}{2\beta}\frac{1}{g_m\mathbf{k}^2 + \mu_z} \tag{17}$$

with

$$\mu_z = a(\omega_c - \omega_0) + 10b\,\langle m_z^2 \rangle_0 + 105c\,\langle m_z^2 \rangle_0^2, \tag{18}$$

where ω_0 is the equilibrium volume per atom.

Fluctuations are dealt with in Gaussian approximation leading to a mode-mode coupling theory which leads to nontrivial self-consistency equations for the temperature dependence of magnetization, volume, mean-square fluctuation amplitudes, thermal expansion, specific heat, susceptibility, etc. We omit the mathematical details here since they have already been presented in Refs. 51–56. The Landau coefficients can be determined nearly unambiguously from the KKR-CPA binding surfaces. They are displayed in Table II (for comparison Table III shows the Landau coefficients for pure Fe and Ni). With this input we can determine the finite-temperature binding surfaces which are displayed in Fig. 10 for the most interesting case corresponding to $x = 0.65$. For this Invar concentration the input data of Table II yield a nonmag-

TABLE II. The set of Ginzburg-Landau coefficients[a] used in the finite-temperature fluctuation theory for different compositions of the alloy Fe_xNi_{1-x}.

System	a	b	c	ω_c	κ	γ	δ
$Fe_{60.0}Ni_{40.0}$	29.5256	−1.5764	0.4119	0.0643	1355.94	−1869.76	4858.70
$Fe_{62.5}Ni_{37.5}$	29.3134	−1.4516	0.3574	0.0731	1353.58	−1701.94	4223.20
$Fe_{65.0}Ni_{35.0}$	29.0076	−1.4443	0.3300	0.0872	1355.32	−1551.37	3589.93
$Fe_{67.5}Ni_{32.5}$	28.8228	−1.3192	0.2859	0.0947	1346.88	−1354.10	2958.04
$Fe_{70.0}Ni_{30.0}$	28.6963	−1.1289	0.2354	0.0982	1346.28	−1173.78	2262.49

[a]Units are chosen so that the magnetization is in units of μ_B/atom and the energy in mRy/atom.

netic ground state lying slightly lower in energy than the magnetic solution. At elevated temperatures $T \approx 50$ K magnetic- and volume-fluctuation amplitudes are larger for the NM (LM) state than for the HM state. Hence the HM state becomes a more stable solution at elevated temperatures due to competition of fluctuations of different phases. This leads to reentrant behavior and a high-temperature ferromagnetic phase. Note that this behavior is limited to a very narrow concentration range in the vicinity of $x = 0.65$. Note also that for $x = 0.65$ one observes spin-glass-like behavior in the real sample at low temperatures due to noncollinear spin arrangements, and not a stable ferromagnetic phase. So this simple fluctuation theory even mimicks details of the low-temperature Fe-Ni phase diagram. However, we must emphasize that the fluctuation theory does not describe a low-temperature spin-glass phase at 65 at.% Fe but a nonmagnetic (NM) state with a local minimum on the $M = 0$ line in Fig. 10(a) having slightly lower energy than the HM state at $M \approx 1.5\mu_B$. The general behavior of binding surfaces with increasing temperature is that each surface elongates vertically and is shifted downwards to the $M = 0$ line within our simple fluctuation scheme. Hence in this particular case, the minimum of the zero-temperature NM state disappears and the HM state is stabilized with increasing temperature.

The behavior of the specific heat is shown in Fig. 11. The onset of magnetism for 65 at.% Fe corresponds to a phase transition and leads to an additional specific-heat jump below T_c [we have used here temperature-dependent cutoffs $q_{m,\omega}(T) = (T/T_c)^{1/3} q_{m,\omega}$ for the momentum summation in order to avoid unphysical heat-capacity behavior at low temperatures; this causes the onset of magnetism to shift to higher temperatures as compared to the results in Fig. 10, where temperature-independent cutoff parameters have been used]. Figure 11(b) shows the reduced specific heat which is obtained from

$$C = \frac{k_B}{12\pi^2}\left(3q_m^3 + 3q_\omega^3\right) - \langle m_z^2\rangle_0 \frac{\partial \mu_z}{\partial T} - \langle m_\perp^2\rangle_0 \frac{\partial \mu_\perp}{\partial T} - \langle \omega^2\rangle_0 \frac{\partial \mu_\omega}{\partial T} \tag{19}$$

by subtracting the first term (μ_z, $\mu_\perp$, and μ_ω are variational fields[54]). It can be seen that $Fe_{67.5}Ni_{32.5}$ and $Fe_{70}Ni_{30}$ show a tendency for magnetic order.

The theoretical specific-heat curves show a jump at T_c, whereas the experimental specific-heat curve for $Fe_{65}Ni_{35}$ does not show any sign of a jump. This shortcoming of our theory is due to the fact that we have no means of dealing with the influence of disorder on the heat capacity at finite temperatures if we use the simple functional form in Eq. (13). This shortcoming could probably be avoided by incorporating the concentration dependence in the functional form and by allowing for concentration fluctuations. An additional problem is connected with the fact that within the finite-temperature fluctuation theory, the magnetic specific heat has a tendency to become negative above T_c, whereas experiment very often shows additional specific heat. In our continuum theory this is connected with the ever growing amplitudes of fluctuations with increasing temperature. As was pointed out by Moriya,[63] the longitudinal spin-fluctuation amplitude should saturate because of the limited number of electrons per atom. This was investigated in detail within a finite-temperature fluctuation theory similar to ours by Mohn and Hilscher.[64] They showed that saturation effects are important and can lead to an additional maximum in the specific heat which lies below T_c.

However, one should add that the specific-heat behavior of Invar alloys is far from being understood. For example, the pseudobinary system $Fe_{50}Ni_xMn_{50-x}$ exhibits anomalously large contributions to the specific heat in the paramagnetic phase for concentrations $0.21 < x < 0.35$ as well as a broad smeared out maxi-

TABLE III. The set of Ginzburg-Landau coefficients of pure fcc Fe and Ni.

System	a	b	c	ω_c	κ	γ	δ
Fcc Fe	28.8670	−0.9510	0.0868	0.28	1280.94	−1301.50	2100.70
Fcc Ni	20.3102	25.0133	−2.8059	−0.80	1144.34	−949.12	562.59

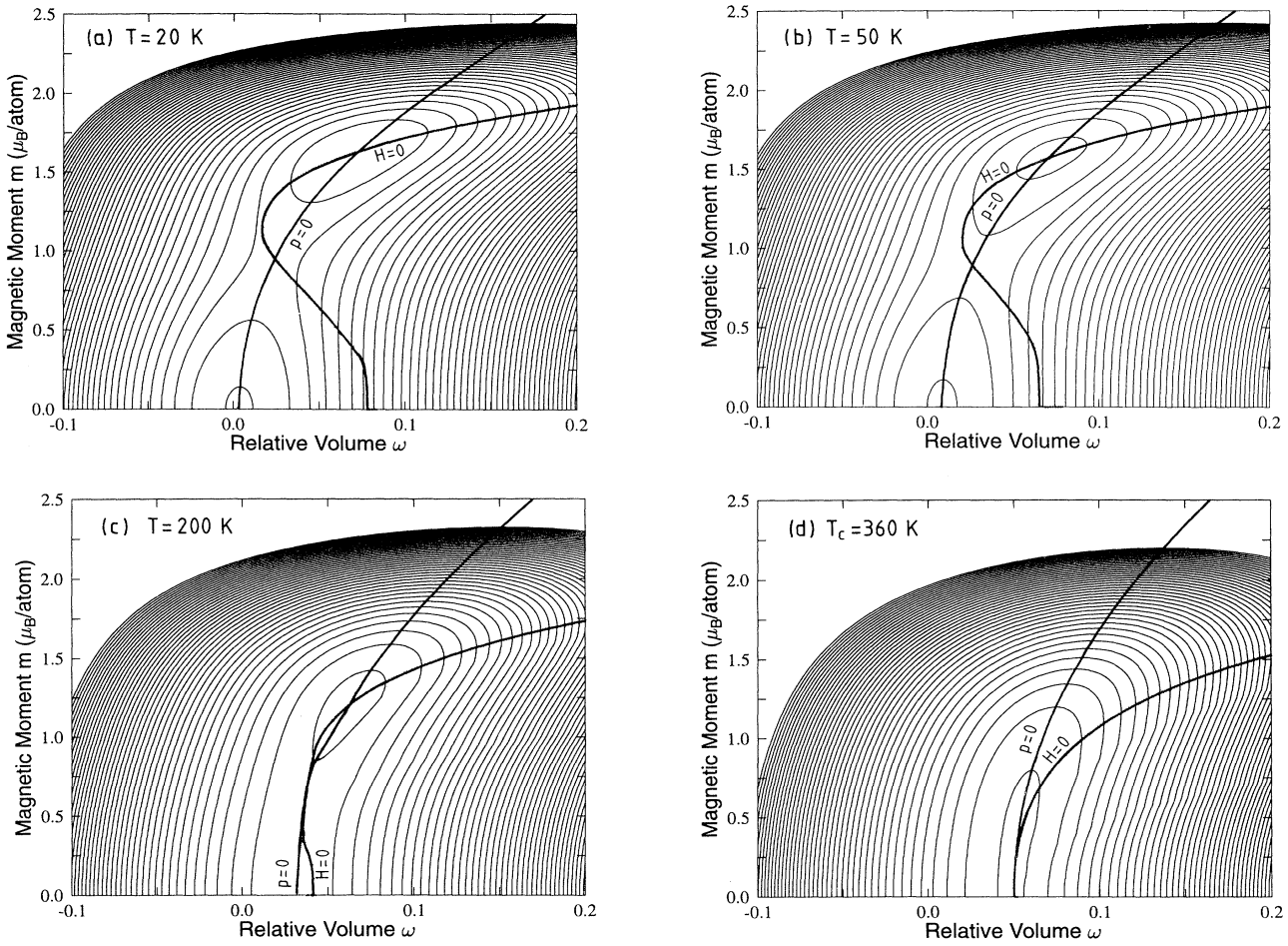

FIG. 10. Binding surfaces of $Fe_{65}Ni_{35}$ as obtained with the finite-temperature fluctuation theory. Contour lines are at 0.5 mRy intervals. Note that in (a) the NM solution is the lowest energy solution at $T = 20$ K, whereas the HM solutions in (b)–(d) become more stable for temperatures $50 < T < T_c = 360$ K. This reentrant behavior exists only in a narrow concentration range at $x = 0.65$ and occurs because the mean-square fluctuation amplitudes are larger at low temperatures for the NM than for the HM solution [compare Fig. 12(a)]. Also shown are the $H = (\partial E/\partial M)_V = 0$ and $p = -(\partial E/\partial V)_M = 0$ lines.

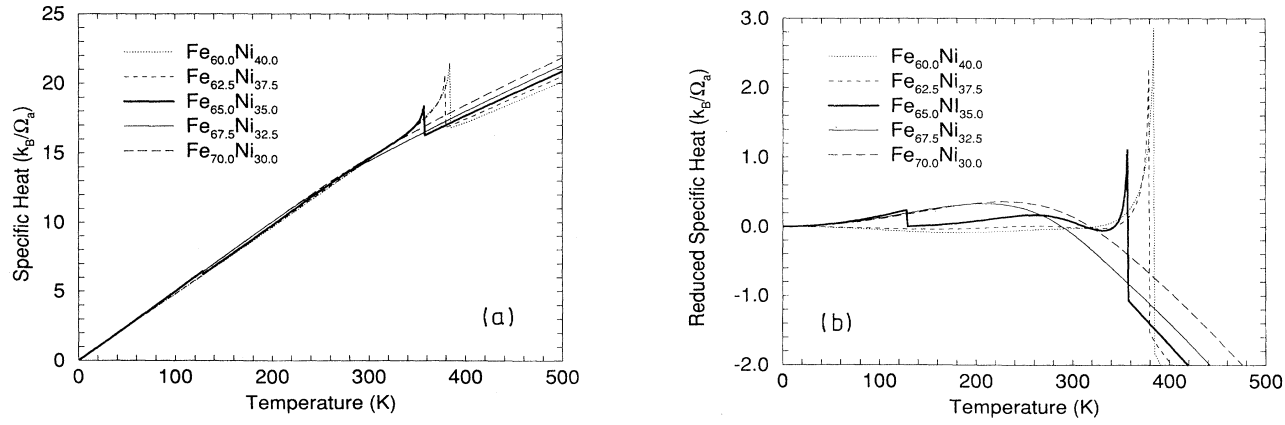

FIG. 11. (a) Behavior of the specific heat as function of temperature for typical Invar concentrations (Ω_a is the atomic volume). Note that for reentrant $Fe_{65}Ni_{35}$ the specific heat has two peaks. (b) Behavior of the reduced specific heat after subtraction of the terms arising from the momentum cutoffs in (19). There is a tendency for $Fe_{67.5}Ni_{32.5}$ and $Fe_{70}Ni_{30}$ to become magnetic.

mum close to T_c.[65] While this maximum still looks like a well pronounced λ anomaly in the case of $Fe_{50}Ni_{50}$ (at $T_c = 765$ K), this anomaly starts to disappear for $Fe_{50}Ni_{40}Mn_{10}$.[2,66] If the transition temperatures of this alloy series fall below 400 K, then even the smeared maximum has disappeared.[67] We refer to Ref. 68 for further discussion of the specific-heat behavior.

In Fig. 12(a) we show the temperature behavior of the HM magnetization and of longitudinal and transverse amplitudes of fluctuation for the NM (dashed lines) and the HM (solid lines) solutions. The amplitudes of fluctuation for the NM (LM) solution look similar to the HM solution with one marked difference, that is, the longitudinal amplitude is considerably larger for the NM case than for the HM case. As discussed above, this destabilizes the nonmagnetic phase at elevated temperatures and leads to reentrant behavior.

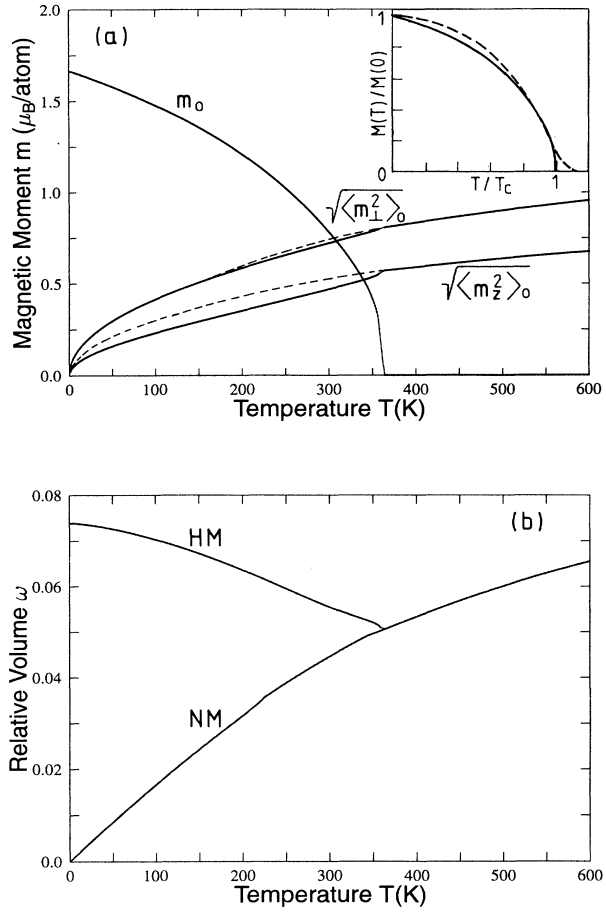

FIG. 12. Temperature dependence of (a) HM magnetization and amplitudes of fluctuations and of (b) HM and NM volumes showing that both join at T_c within the finite-temperature fluctuation theory. Dashed curves show the fluctuation amplitudes for the NM solution. The inset compares theoretical (solid line) and experimental (dashed line) (Ref. 70) magnetization curves; apart from the low-temperature behavior there is rather good agreement between theory and experiment.

The saturation magnetization in Fig. 12(a) behaves qualitatively as experimentally observed. The calculated curve lies well below the Brillouin curve. The low-temperature behavior is wrong since contributions from collective excitiations (spin waves) are not taken into account well enough in the finite-temperature spin-fluctuation theory. Since cutoff parameters for momentum integration are not of optimum choice, the Curie temperature is only 360 K, whereas experiment gives 548 K.[69] Yet it is interesting to compare the overall behavior of experiment and theory. The inset shows the scaled experimental data (dashed line)[70] and the scaled theoretical magnetization curve (solid line). Apart from the low-temperature deviation there is good agreement between the two curves.

It is also interesting to compare results for the fluctuation amplitudes, $\langle \mathbf{m}^2 \rangle_0$ with neutron-scattering data for $Fe_{65}Ni_{35}$ in the paramagnetic phase at $T = 1.25\,T_c$.[71] The mean-square amplitude of fluctuation (*equal-time correlation function*) is obtained from the measured constant $\mathbf{q}$ spectrum using the relationship[72]

$$\langle \mathbf{m}^2(\mathbf{q}) \rangle = 6 \int_{-\infty}^{\infty} d\omega\, S(\mathbf{q}, \omega) \tag{20}$$

$$= \frac{I(\mathbf{q})}{0.0485\, f^2(\mathbf{Q})\, e^{-2W}}, \tag{21}$$

where $S(\mathbf{q}, \omega)$ is the scattering function; $I(\mathbf{q})$ is the integrated intensity and $f(\mathbf{Q})$ the magnetic form factor. It is interesting to note that $\langle \mathbf{m}^2(\mathbf{q}) \rangle$ is isotropic in the measured $\mathbf{q}$ range. In order to make comparison with theory the authors use

$$\langle \mathbf{m}^2(0) \rangle = 3 k_B T\, \chi(0), \tag{22}$$

where $\chi(0)$ is the uniform susceptiblitiy, and the molecular field result for localized moments (or local-moment limit of the band theory[62]),

$$\langle \mathbf{m}^2(\mathbf{q}) \rangle \approx 3 k_B T\, \chi(\mathbf{q}, \omega = 0) = \frac{\langle \mathbf{m}^2(0) \rangle}{1 + \dfrac{\hbar \omega_{\mathbf{q}} \langle \mathbf{m}^2(0) \rangle}{3 k_B T (g \mu_B)^2 S}} \tag{23}$$

with the low-temperature spin-wave energy $\hbar\omega_{\mathbf{q}}$. The left part of Eq. (23) corresponds to the classical fluctuation-dissipation theorem which is assumed to hold in the high-temperature limit $\hbar\omega / k_B T \ll 1$. The quantity $\langle \mathbf{m}^2(0) \rangle$ is obtained from the static susceptibility and the spin-wave dispersion from $\hbar\omega_{\mathbf{q}} = D\mathbf{q}^2(1 - \beta \mathbf{q}^2)$ with $D = 143$ meV Å^2 and $\beta = 0.12$ Å^2.[73] The authors stress that although there is no adjustable parameter in this calculation, the agreement with experiment is perfect.[71]

Figure 13 shows the amplitudes of spin fluctuations $\langle \mathbf{m}^2(\mathbf{q}) \rangle$ for the three systems $Fe_{65}Ni_{35}$,[71] bcc Fe,[74] and fcc Ni.[75] The solid lines are curves fitted to experiment by using relation (23) with parameters for the spin-wave spectra from Table IV.[71] The fit is perfect in the case of $Fe_{65}Ni_{35}$ and Ni, while for bcc Fe the fitted curve behaves reasonably only for lower q values. The figure shows that spin-fluctuation amplitudes are largest for the Invar alloy. For comparison we show our theoretical re-

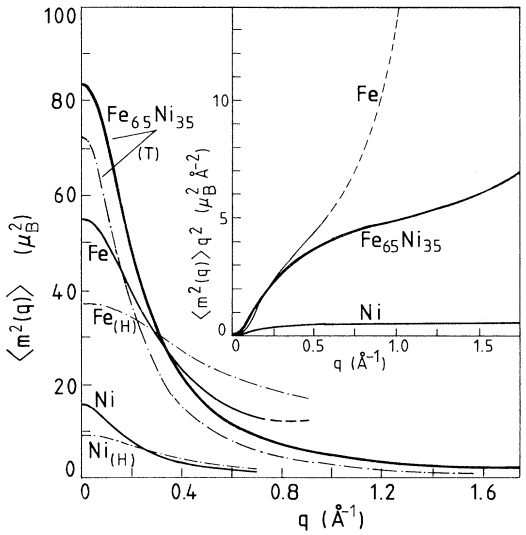

FIG. 13. The amplitude of the spin fluctuation (*equal-time correlation function*) $\langle \mathbf{m}^2(\mathbf{q}) \rangle$ for $Fe_{65}Ni_{35}$ along [100] (Ref. 71), bcc Fe along [110] (Ref. 74), and for fcc Ni along [111] (Ref. 75). The solid curves are fits to the experimental data by using Eq. (23) with the parameters of Table IV. The dashed dotted curve for $Fe_{65}Ni_{35}$ denoted by (T) is our theoretical result, the curves marked by (H) stem from Hasegawa. (Refs. 76 and 77). The inset shows the (experimental) amplitude of fluctuation multiplied by the phase factor q^2 for $Fe_{65}Ni_{35}$, Fe, and Ni, respectively. The result for Fe for larger q values is probably an overestimation (dashed line).

sult for $Fe_{65}Ni_{35}$ and the theoretical result for Fe and Ni taken from Hasegawa.[76,77] The theoretical result for $Fe_{65}Ni_{35}$ agrees qualitatively with experiment. The theoretical curves in the case of Fe and Ni do not decay fast enough for small q.

The inset shows the experimental fluctuation amplitudes multiplied by the phase space factor q^2. This phase factor appears when integrating the amplitudes over the first Brillouin zone. There is a continuous increase in all three cases showing that fluctuations with large q values make very important contributions. We do not observe a peak in $q^2\langle \mathbf{m}^2(\mathbf{q}) \rangle$ in any of these cases in contrast to earlier experimental data of neutron scattering on paramagnetic iron.[78] These authors observe a peak structure at $q = 0.4$ Å^{-1} from which they deduce a typical wavelength for *spin waves* of the order of 16 Å. This strong short-range magnetic order in the paramagnetic phase has been questioned arguing that the energy window in the experiments may not be sufficient to include the whole magnetic scattering (for further discussion see Ref. 76).

It is quite interesting to deduce the effective moment, the correlation length, and the local moments for the case of $Fe_{65}Ni_{35}$ from the experimental data by using

$$\begin{aligned} \langle \mathbf{m}^2(\mathbf{q}) \rangle &= \frac{\mu_{\text{eff}}^2(T)\,T}{T - T_c} \quad \text{for } \mathbf{q} = 0 \text{ and } T \to \infty, \\ &= \frac{\mu_{\text{eff}}^2(T)\,T}{T - T_c} \frac{1}{1 + \xi q^2} \quad \text{for } \mathbf{q} \to 0, \\ &= \mathbf{m}_{\text{loc}}^2 \quad \text{for } \mathbf{q} \to q_{\text{BZ}}. \end{aligned} \tag{24}$$

This yields for $T/T_c = 1.25$ the following values: $\mu_{\text{eff}} = 4.1\mu_B$ [which is larger than the ideal paramagnetic scattering value being $\mu_{\text{eff}}(T = \infty) = 3.3\mu_B$], $\xi = 4.32$ Å [equating (23) and (24)], and $m_{\text{loc}} = 1.50\mu_B$ (at $q = q_{\text{BZ}}$). This gives $m_{\text{loc}}^{\text{Fe}} = 2.0\mu_B$ if we assume that Ni still has its full moment, $m_{\text{loc}}^{\text{Ni}} = 0.57$. It is also interesting to calculate in the same way the correlation lengths of Fe and Ni at $T/T_c = 1.25$. They are $\xi_{\text{Fe}} = 3.16$ Å and $\xi_{\text{Ni}} = 5.06$ Å being considerably larger than the values calculated by Hasegawa ($\xi_{\text{Fe}} = 1.25$ and $\xi_{\text{Ni}} = 2.6$ Å).[76,77]

In order to compare our fluctuation amplitudes in Fig. 12(a) with Ref. 71, we integrate the momentum dependence of the experimental values over the whole Brillouin zone with the help of Eq. (23) giving $m_{\text{loc}}(T/T_c = 1.25) = 4.1$ which is larger than the value obtained from the edge of the Brillouin zone given above ($m_{\text{loc}} = 1.50$). This difference might be connected with the concept used in Ref. 71 to use the relation (23) with an expansion of the low-temperature spin-wave dispersion as input, at very elevated temperatures in the paramagnetic region. We think that this overestimates a bit the scattering contributions coming from the high-momentum area. This overestimation is clearly visible in Fig. 13 for the case of Fe, where it leads to unreasonable results for the high-momentum states. Therefore, the value $m_{\text{loc}} = 1.50$ deduced from experiment for the case of $Fe_{65}Ni_{35}$ is much more reliable. This value compares fairly well with our result of $1.04\mu_B$ for the sum of fluctuation amplitudes at $T = 1.25\,T_c$ in Fig. 12(a) in spite of the fact that our fit of T_c is poor.

The temperature variation of the volume expansion and contraction of the NM and HM state is shown in Fig. 12(b), respectively. Note that the different volumes approach each other and merge at T_c. With respect to the thermal expansion this means that there is a gradual

TABLE IV. Parameters for the calculation of the amplitude of fluctuation in Eq. (23) obtained from measurements of the spin-wave dispersion, susceptiblity and magnetization (see Ref. 71 for details and references to experimental work).

System	D (meV Å^2)	β (Å^2)	$\langle \mathbf{m}^2(0) \rangle$ (μ_B^2)	S
$Fe_{65}Ni_{35}$	143	0.12	84.0	0.91
Fe (3.5% Si)	270	0.70	55.0	1.11
Ni	400	0.00	15.5	0.30

transition from the low-temperature NM behavior to the high-temperature HM behavior.

The thermal-expansion coefficient which is easily obtained from the derivative of the relative volume change displayed in Fig. 12(b), does not perfectly agree with experiment. But this is clear since details of the true thermal-expansion curve are connected with important charge transfers in the temperature range $0 < T < T_c$ which is beyond the scope of a Landau description with temperature-independent parameters. The thermal-expansion coefficient obtained here first increases at low temperatures in the nonmagnetic state, then remains approximately constant in the transition region to the ferromagnetic phase, and finally decreases up to T_c in the ferromagnetic state.

In this section we have shown that the zero-temperature KKR-CPA FSM binding surfaces of disordered alloys are equally well suited to serve as input for the finite-temperature fluctuation theory as the surfaces obtained by ASW-FSM calculations for ordered systems. A close inspection of Table II shows that a change of concentration x towards the more Fe-rich side changes the Landau parameters in a systematic way; a and c decrease while b increases resulting in weaker magnetism. Also the elastic coefficients show a systematic trend. For example, the coefficient κ being proportional to the bulk modulus, softens considerably by going from the Ni-rich side (with strong ferromagnetism) to the Fe-rich side with weak ferromagnetism in the fcc structure. A closer inspection shows that the change of parameters scales in a nontrivial way with concentration when going from the magnetic to the nonmagnetic ground state.

Altogether one may say that the finite-temperature fluctuation theory describes qualitatively correct some of the Invar behavior of $Fe_{65}Ni_{35}$. The finite-temperature magnetic binding surfaces in Figs. 10(a)–10(d) can be considered as a central result. We believe that they show the Invar behavior at finite temperatures. For example, Figs. 10(c) and 10(d) show how the region of minimal energy around the ferromagnetic ground state becomes very elongated with negative magnetic anharmonicity. A characteristic feature is also that the Fe-Ni system can go from one state to many in energy close lying to other states which can have quite different magnetic moments due to local fluctuations of temperature, volume or concentration. Of course, our finite-temperature fluctuation theory can not describe the resonant coupling of electronic transitions to phonons and the pseudogap formation. We have only a coarse-grained picture of the impact of spin and volume fluctuations on thermodynamic variables. Other drawbacks are mainly connected with missing quantum-mechanical aspects at low temperatures.[54] An artifact is connected with the nature of the phase transition itself which turns out to be of first order in any self-consistent spin-fluctuation theory based on Gaussian fluctuations. There is no simple way to avoid this since the Gaussian approximation violates the fluctuation-dissipation theorem.[54,79] More refined spin-fluctuation theories based on the Hubbard model[62] still show this artifact when they are based on the Gaussian method.

V. STRUCTURAL BINDING SURFACES OF Fe_xNi_{1-x}

The phase diagram of Fe_xNi_{1-x} in Fig. 1 shows that the onset of martensitic transformation is just on the borderline of the magnetovolume instability. Another characteristic feature is that the Curie temperature as well as the transition temperatures for the structural transformation considerably decrease when approaching the critical concentration $x \approx 0.70$. Similar behavior is observed for ordered and disordered $Fe_{72}Pd_{28}$ and $Fe_{72}Pt_{28}$ (where, however, the low-temperature magnetic moment does not change much in the instability region). Therefore, the question arises whether Invar on the γ side and the formation of martensite on the α side have some common origin. One common feature seems to be that on both sides (γ and α) of the structural transition we find magnetic order. On the α side the less close-packed low-temperature bcc structure (compared to the more close-packed high-temperature γ phase) seems to be stabilized by ferromagnetic order since usually the fcc structure is realized in the ground state. In order to check this, we made some preliminary investigations. For example, the influence of local distortions along the Bain path in Fe_3Ni and its connection with the martensitic transition was discussed in Refs. 6, 7, and 59 on the basis of ASW-LDA total-energy calculations. This served as input for a Landau formulation which contains symmetry adapted strain fields as well as the fields $(\mathbf{m}, \omega)$. This allowed us to establish a structural binding surface for the Fe-Ni system which displayed quite nicely on one and the same surface two local minima belonging to the fcc and the bcc structure, respectively.

Unfortunately, in order to obtain the $(r_{WS}, c/a)$ binding surface from the Landau-Ginzburg Hamiltonian, we had to assume how magnetism changes on the surface. For simplicity we used for each fixed r_{WS} radius the same change as obtained from the ASW calculation. This procedure produced a rather deformed binding surface. Therefore, we have recalculated the structural binding surface with the ASW method [see Fig. 14(g)]. Compared to the surface obtained with the effective Landau Hamiltonian,[59] we now find a very unstable fcc state having a very shallow minimum. We also observe that the position of the bcc minimum is not exactly at $c/a = 1/\sqrt{2}$. We attribute this to the fact that because of two atomic species distributed regularly, $c/a = 1/\sqrt{2}$ does not correspond to a true bcc phase.

Of particular interest are now the KKR-CPA binding surfaces, since we know that, for example, $Fe_{75}Ni_{25}$ has a nonmagnetic fcc ground state while Fe_3Ni has a magnetic fcc ground state (see Fig. 4). Figure 14 shows the structural binding surfaces of Fe_xNi_{1-x} for the interesting range of concentrations, where the magnetic moment collapses and where martensite forms. In Figs. 14(a), 14(c), and 14(e), the magnetic moment was allowed to relax at each point of the surface corresponding to $H = 0$, while in (b), (d), and (f) the magnetic moment was constrained to have the value $M = 0$ everywhere by using the FSM procedure. The results show that obviously in the absence of magnetism the ground state is realized in

the fcc structure in this concentration range. Allowing for magnetic order destabilizes the fcc structure and results in a magnetic bcc ground state. By comparing the energetic scenario in Figs. 4 and 14 one finds that in the instability region magnetic and structural excitation energies seem to be of equal importance. What we also find interesting is connected with the ground-state volumes of the HM fcc and bcc states. They approximately are of equal magnitude, the difference being of the order of 0.1% for each concentration.

Let us now concentrate on $x = 0.75$. The corresponding $(r_{\mathrm{WS}}, c/a)$ binding surface of $Fe_{75}Ni_{25}$ is shown in Fig. 14(e). It is different from the stoichiometric case in (g) with respect to the following features. (i) The surface exhibits now two minima and a saddle point. On the $c/a = 1$ fcc line we have the HM saddle point at

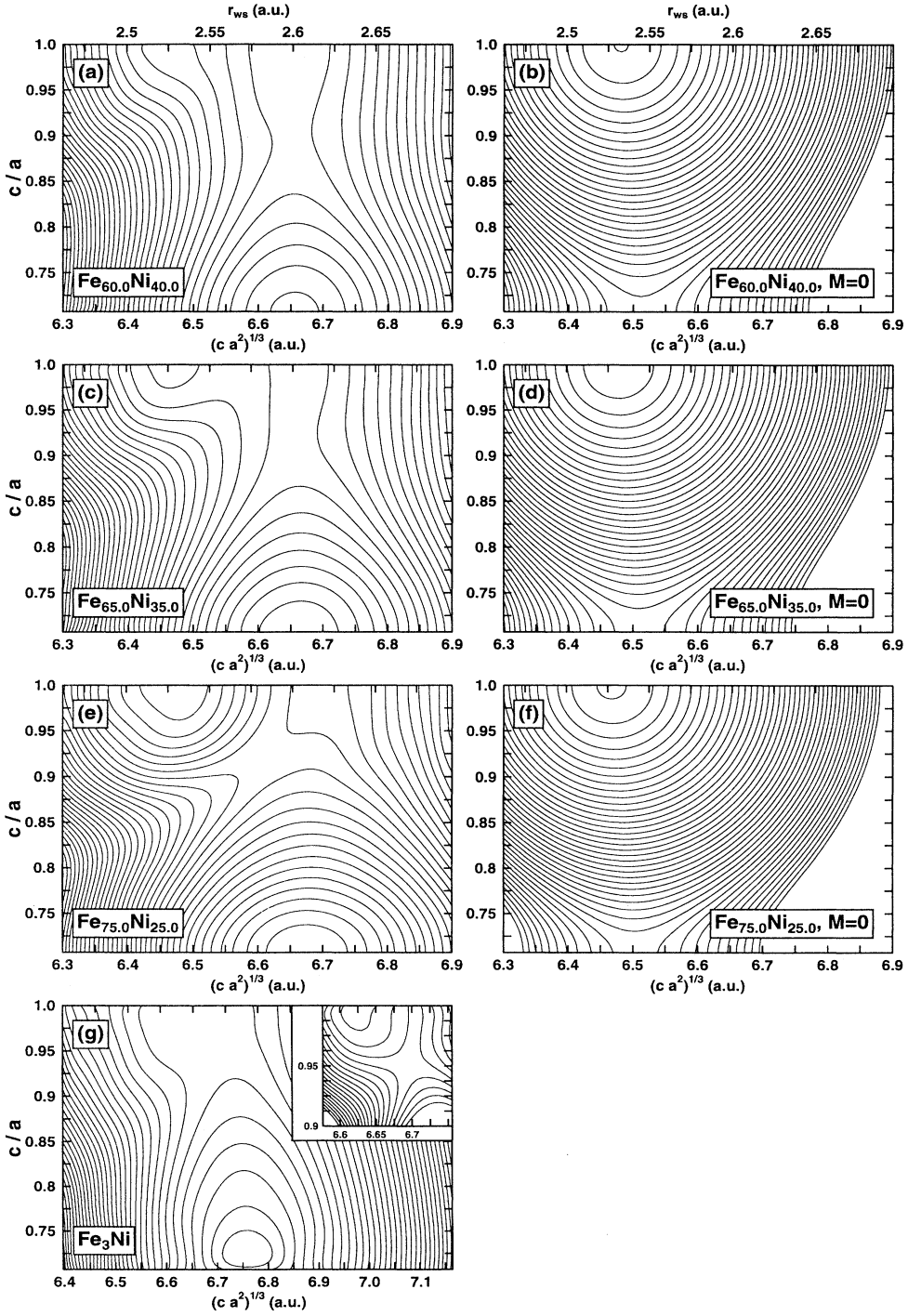

FIG. 14. Structural binding surfaces of Fe_xNi_{1-x} for (a) $x = 0.60$, (c) $x = 0.65$, and (e) $x = 0.75$ as obtained from the KKR-CPA calculation, and (g) Fe_3Ni as obtained from the ASW calculation; (b), (d), and (f) show FSM-KKR-CPA results with $M = 0$ everywhere on the surface. $c/a = 1$ and $c/a = 1/\sqrt{2}$ corresponds to the fcc structure and bcc structure, respectively. Contour lines are at 0.5 mRy intervals; in the inset of (g) contour lines are at 0.05 mRy intervals. (a), (c), (e), and (g) have a ferromagnetic bcc ground state, while the nonmagnetic surfaces, (b), (d), and (f), show a very stable minimum at the fcc equilibrium volume. Nonmagnetic and LM states are separated from the HM region by a first-order transition line which extends from $c/a = 1$ into the surface, and which is responsible for the rather deformed contour lines in the case of $Fe_{75}Ni_{25}$.

$r_{WS} = 2.61$ corresponding to the HM state on the magnetic binding surface in Fig. 4(g), and a shallow nonmagnetic minimum at $r_{WS} = 2.53$ corresponding to the NM state in Fig. 4(g), while the bcc phase has a rather deep minimum at $r_{WS} = 2.61$. HM saddle point and NM minimum are connected by the $H = 0$ line in Fig. 4(g), while they are connected by the $c/a = 1$ path in Fig. 14(e). (ii) The bcc minimum is now at $c/a = 1/\sqrt{2}$ as expected, since CPA forms one effective atom giving rise to a binding surface which should have its minimum at a high-symmetry point. (iii) The particular new feature is, as compared to our old results, that the Bain path would now connect the bcc state and this fcc saddle point with practically no volume change, while for Fe_3Ni this would result in a 2.02% contraction when going from bcc to fcc. (iv) Note also that the disordered $Fe_{75}Ni_{25}$ bcc ground state has a lower volume compared to the ordered phase.

Figures 15–17 show energy versus the c/a ratio for $x = 0.60$, 0.65, and 0.75 and constant volumes. The all over behavior of the $E(c/a)$ curves at fixed volume can be explained as follows. The total energy can be decomposed into the band energy

$$E_B = \int_{E_0}^{E_F} d\varepsilon N(\varepsilon)\,\varepsilon, \tag{25}$$

where E_0 is the bottom of the valence band and $N(\varepsilon)$ is the valence electron density of states, the electrostatic Ewald energy

$$E_{EW} = (1.8 - \alpha_M)\frac{q^2}{r_{WS}}\left(\frac{\Omega_{WS}}{\Omega_{MT}}\right)^2 \tag{26}$$

and contributions which depend only on volume. Ω_{WS} and Ω_{MT} is the volume of the Wigner-Seitz and the muffin-tin sphere, respectively, and q the charge inside the Wigner-Seitz sphere minus the charge inside the nonoverlapping muffin-tin sphere; α_M is the Madelung constant (for further discussion we refer to the literature[80]). The band energy essentially follows the total energy for $1/\sqrt{2} < c/a < 1$ and decreases outside of this region, while the electrostatic energy is small for $1/\sqrt{2} < c/a < 1$ but then increases rapidly, because electrostatics makes so highly distorted fct and bct lattices very unfavorable. So the increase of the energy for

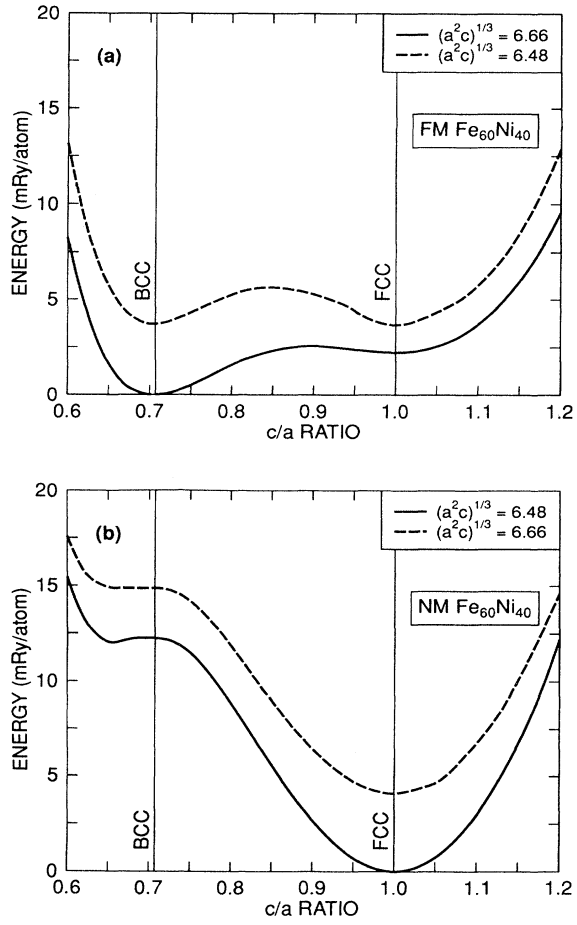

FIG. 15. Energy along the Bain path for (a) ferromagnetic and (b) nonmagnetic $Fe_{60}Ni_{40}$ for two different volumes.

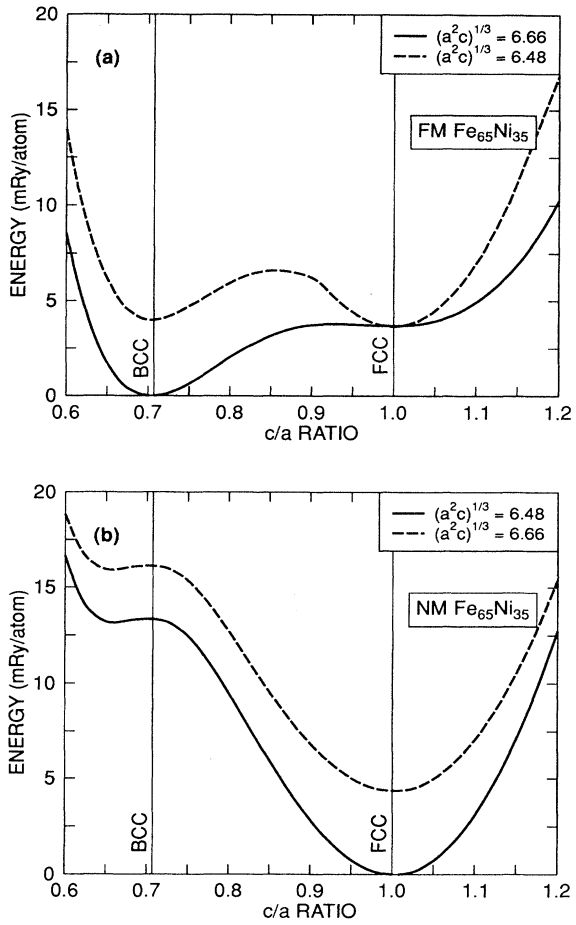

FIG. 16. Energy along the Bain path for (a) ferromagnetic and (b) nonmagnetic $Fe_{65}Ni_{35}$ for two different volumes.

$c/a < 1/\sqrt{2}$ and $c/a > 1$ is of electrostatic origin.

Figures 14(a), 14(c), and 14(e) and Figs. 15–17 show that the energy difference between the HM fcc and HM bcc state decreases with decreasing Fe concentration. In our calculation, the bcc state is stable down to $x \approx 0.55$ (see also Fig. 3). This is in contrast to the experimental phase diagram in Fig. 1, where the bcc structure is no longer stable for $x < 0.70$. However, one should be cautious when comparing KKR-CPA energies for different c/a ratios. Since the KKR-CPA code does not contain nonspherical potentials, it is suitable for cubic crystals (fcc, bcc), but for $c/a \neq 1/\sqrt{2}$ or 1, tetragonal symmetry is present. Because nonspherical potentials have been neglected, we estimate the error to be of the order of ± 2 mRy for the total energy differences. A shift of 2 mRy of the energy difference $E_{\rm fcc} - E_{\rm bcc}$ in favor of the fcc structure in Fig. 3 would give a much better agreement between the experimental and theoretical phase diagram. We think that in spite of this error bar, one may say that magnetic and structural excitation energies are of equal magnitude in the instability region and that their coupling at finite temperatures might constitute a link between Invar and martensite.

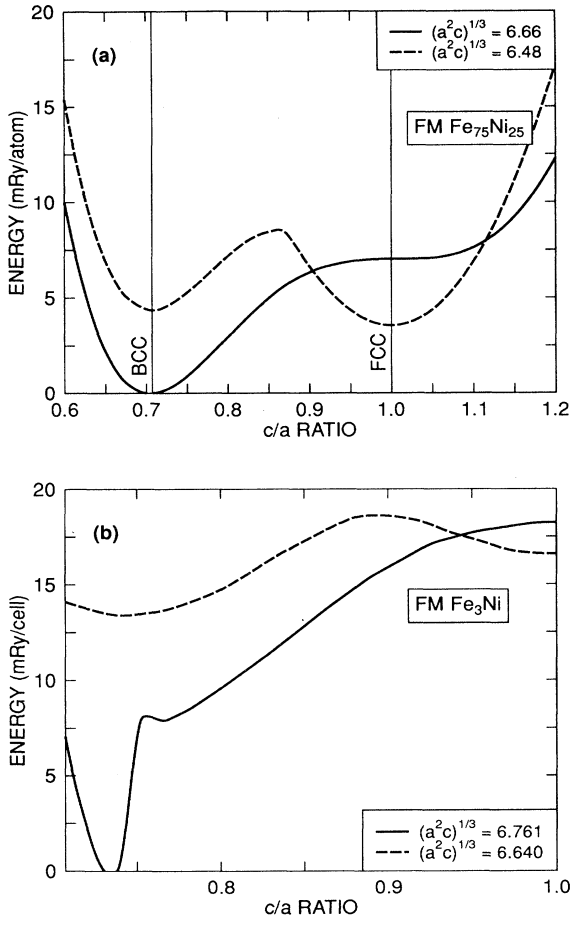

FIG. 17. Energy along the Bain path for (a) ferromagnetic $Fe_{75}Ni_{25}$ and (b) ferromagnetic Fe_3Ni.

In order to illustrate this mutual influence of magnetic and structural excitation energies in short terms, let us consider the cases $x = 0.65$ and 0.75. $Fe_{65}Ni_{35}$ is an fcc Invar alloy which can be characterized at zero temperature by the magnetovolume instability in Fig. 5(b) occuring at a lower volume than the equilibrium volume.[35] The energy difference $E_{\rm NM} - E_{\rm HM}$ is smaller than 1 mRy. The closeness of the martensitic transformation can be seen in Fig. 16(a). The fcc HM state has a very shallow minimum which leads to an energy barrier between the fcc and bcc structure being also smaller than 1 mRy. Hence competing effects may occur at finite temperatures due to interacting magnetic, volume, and tetragonal (shear) fluctuations leading to the formation of austenite or martensite embryos near nucleation centers. Figure 16(b) shows the rather large energy difference between the fcc and the bcc structure in the absence of magnetic order (see also Table V for energy and magnetic-moment values). KKR-CPA results for $Fe_{75}Ni_{25}$ show that for this concentration the bcc structure has become very stable. The gain in energy due to the formation of the bcc structure is of the order of 7 mRy/atom. Here again magnetism is necessary to stabilize the bcc phase, the energy difference between FSM $M = 0$ bcc and $M \neq 0$ is of the order of 17 mRy. As already stated, for the fcc structure disorder is important leading to a nonmagnetic ground state. Figure 5(d) shows that for larger Fe concentrations the Invar effect of the magnetic fcc alloys disappears and that instead fcc Anti-Invar characteristics appear with a magnetovolume instability occuring under lattice expansion. The energy barrier between the HM metastable state and the NM ground state is also of the order of 1 mRy.

In Table V we have also listed calculated values for the bulk modulus B and the elastic constant C' given by

$$B = \frac{1}{3}(c_{11} + 2c_{12}) = V\left(\frac{\partial^2 E}{\partial V^2}\right)_{c/a,M}, \tag{27}$$

$$C' = \frac{1}{2}(c_{11} - c_{12}) = \frac{1}{V}\left(\frac{\partial^2 E}{\partial (c/a)^2}\right)_{V,M}. \tag{28}$$

For those cases, where comparison with experiment is possible, we do not find very good agreement between calculated and experimental values. For example, the calculated value for the bulk modulus B and the shear constant C' in the case of $Fe_{65}Ni_{35}$ (HM fcc ground state) is 22.588 and 4.908 (10^{11} dyn/cm^2), respectively, while ultrasonic measurements yield 13.017 and 1.615 (10^{11} dyn/cm^2) at 4.2 K. However, we would like to point out that all elastic constants of $Fe_{65}Ni_{35}$ show an increase at very low temperatures with some tendency to approach their extrapolated high-temperature values (see Ref. 81 for details). This would give a much better agreement between experiment and theory. In this context one should point out that there are differences between ultrasonic measurements and inelastic neutron-scattering results. For example, in inelastic neutron scattering, the softening in the longitudinal mode is not observed, neither in the FeNi nor in the FePt system, i.e., the longitudinal elastic constant C_L (and also the bulk modulus) is larger than the ultrasound value. For the case of $Fe_{65}Ni_{35}$ neutron scattering leads to $B = 19.8 \times 10^{11}$ dyn/cm^2 which

is much closer to our theoretical value (this value can be derived from the discussion in Ref. 1). The negative values for C' in Table V obtained in the FSM ($M = 0$) calculation for the bcc structure are connected with the bcc saddle point instead of a local minimum [see Figs. 14(b), 14(d), and 14(f)]. Negative values for C' are also obtained for the ferromagnetic cases, for example, C' is negative in a rather wide region separating the HM fcc and HM bcc local minima on the binding surfaces in Figs. 14(a), 14(c), 14(e), and 14(g). This may indicate that very small shear deformations near imperfections could suffice to destabilize spontaneously the fcc or bcc crystal structure. We also think that the decrease of magnetic order (as observed from the lowering of the Curie temperature) when approaching the martensitic transition is important, since the release of magnetic energy might help to overcome the high strain energies which exist due to the formation of martensitic plates in the host.

This discussion shows that the Invar region can be considered as the *premartensitic region* of the fcc→bcc transformation at either zero temperature or at decreasing temperature for concentrations $x < 0.70 - 0.75$ in Fe_xNi_{1-x}. The discussion also shows that the scenario of excitations involving magnetic, structural or mixed ones is rather rich and that competing interactions with small energy differences determine which structure and which magnetic moment is stable at which concentration. For a more detailed discussion of the influence of structure, magnetism, and bonding one would need to discuss the spectral function $A(\mathbf{k}, E)$ for energies close to E_F and for different concentrations in addition with a detailed study of partial pressures for the distorted and the undistorted lattice at finite temperatures. In addition one would need the explicit concentration, volume, and strain dependence of the effective exchange parameters. As already mentioned, this calculation, in particular the evaluation of the effective interatomic exchange potentials, is left for the future. But even without these calculations we have gained some insight into the interrelation of Invar behavior and associated structural instabilities in magnetic transition-metal alloys.

One should add that there are many other theoretical investigations of structural instabilities in Invar alloys. In some work it is emphasized that the instability is of magnetic origin and can be understood on the basis of an anomalous exchange driven instability which can be derived from the localized moment model[82,83] or the itinerant model.[84] We believe that this aspect is very important but would like to add that the finite-temperature martensitic transformation will involve the dynamic modes of specific polarizations which couple most to local changes of charge and spin. This can be deduced from our microscopic investigations.[6,7,59]

TABLE V. Calculated binding energy E (Ry/atom), magnetic moment M (μ_B/atom), bulk modulus B (10^{11} dyn/cm^2), and elastic constant C' (10^{11} dyn/cm^2) for given lattice constant a (a.u.).

	$Fe_{55}Ni_{45}$	$Fe_{60}Ni_{40}$	$Fe_{65}Ni_{35}$	$Fe_{75}Ni_{25}$
HM Bcc (a)	6.648	6.655	6.666	6.673
E	−2764.029 782 1	−2739.251 009 6	−2714.472 328 0	−2664.915 232 7
M	1.660	1.758	1.851	2.025
B	23.480	23.480	23.516	24.160
C'	4.788	10.496	14.700	17.580
HM Fcc (a)	6.640	6.648	6.657	6.690
E	−2764.028 838 5	−2739.248 776 1	−2714.468 629 8	−2664.908 198 1
M	1.603	1.681	1.764	1.859
B	24.760	24.332	22.588	19.460
C'	0.956	2.856	4.908	1.199
LM Fcc (a)	6.450	6.480	6.477	6.469
E	−2764.025 950 7	−2739.247 324 3	−2714.468 660 2	−2664.911 672 2
M	0.044	0.105	0	0
B	33.067	33.163	29.996	29.660
C'	6.199	6.898	8.200	7.048
FSM $M = 0$				
Bcc (a)	6.515	6.510	6.505	6.503
E	−2764.015 092 0	−2739.235 208 8	−2714.455 449 1	−2664.896 282 2
B	27.296	27.776	27.784	28.760
C'	-23.512	-27.620	-31.752	-41.360
FSM $M = 0$				
Fcc (a)	6.486	6.480	6.477	6.469
E	−2764.026 128 7	−2739.247 328 3	−2714.468 660 2	−2664.911 672 2
B	28.172	28.652	28.916	29.692
C'	11.204	12.244	13.176	15.424

VI. CONCLUSIONS

We have discussed the influence of disorder on magnetic and structural instabilities in the Fe-Ni system on the basis of KKR-CPA FSM calculations. The results show that atomic disorder is important and cannot be neglected in calculations of magnetic, Invar or martensitic properties of transition-metal alloys. Calculations show that disordered Fe_xNi_{1-x} becomes nonmagnetic at a critical concentration in the Invar region in accordance with experiment. Although calculations for other Invar systems like $Fe_{72}Pt_{28}$ which in contrast to the Fe-Ni system can be prepared as ordered and disorderd sample, have only started, we expect that the KKR-CPA method can also in this case account for the marked differences between the physical properties of ordered and disorderd samples. Furthermore it has been shown that magnetism is of crucial importance for both, the Invar properties as well as the formation and stabilization of martensite. Typical energy differences like $|E_{\mathrm{NM}} - E_{\mathrm{HM}}|$ and $|E_{\mathrm{fcc}} - E_{\mathrm{bcc}}|$ become smaller and smaller when approaching the collapse of the magnetic moment. We think that this explains qualitatively the strong decrease of Curie, austenite and martensite transformation temperatures as function of the concentration. The KKR-CPA calculations of the magnetic binding surfaces have been extended to finite temperatures with help of a fluctuation theory. Although disorder is not correctly taken into account in the most simple version of the fluctuation theory, results for magnetization, amplitude fluctuations, volume changes, and thermal expansion look reasonable and describe qualitatively the experimental data.

ACKNOWLEDGMENTS

One of us (P.E.) would like to thank Professor Wassermann and Professor Acet for many valuable discussions. This work was supported by the Deutsche Forschungsgemeinschaft through SFB 166.

*Electronic address: janne@thp.uni-duisburg.de
†Electronic address: he@gaia.phys.chemie.uni-muenchen.de
‡Electronic address: akai@phys.wani.osaka-u.ac.jp
§Electronic address: entel@thp.uni-duisburg.de
**Permanent address: Department of Physics, Kakatiya University, Warangal 506 009, India.

[1] *ISOMES'89, Proceedings of the International Symposium on Magnetoelasticity and Electronic Structure of Transition Metals, Alloys, and Films*, edited by E. F. Wassermann, K. Usadel, and D. Wagner [Physica B **161** (1989)].
[2] E. F. Wassermann, Phys. Scr. T **25**, 209 (1989).
[3] E. F. Wassermann, in *Ferromagnetic Materials*, edited by K. H. J. Buschow and E. P. Wohlfarth (Elsevier, Amsterdam, 1990), p. 237.
[4] E. F. Wassermann, J. Magn. Magn. Mater. **100**, 346 (1991).
[5] E. F. Wassermann, Europhys. News **22**, 150 (1991).
[6] P. Entel, E. Hoffmann, P. Mohn, K. Schwarz, and V. L. Moruzzi, Phys. Rev. **47**, 8706 (1993).
[7] E. Hoffmann, P. Entel, K. Schwarz, and P. Mohn, J. Magn. Magn. Mater. **140-144**, 237 (1995).
[8] J. Kaspar and D. R. Salahub, Phys. Rev. Lett. **47**, 54 (1981).
[9] Th. Kleemann, R. Jungblut, J. Dresselhaus, and E. Kisker, in *Metallic Alloys, Experimental and Theoretical Perspectives*, edited by J. S. Faulkner and R. D. Jordan (Kluwer, Dordrecht, 1994), p. 17.
[10] For a discussion of different interpretations of the temperature variation of exchange splitting in Fe in connection with the consideration of different time scales for finite temperature itinerant magnetism see, for example, W. Gudat, J. Appl. Phys. **57**, 3609 (1985); M. B. Sterns, *ibid.* **57**, 3030 (1985); H. Capellmann, J. Phys. (Paris) Colloq. **43**, C7-351 (1982).
[11] General aspects of local environment effects on the magnetization versus concentration curve of transition-metal alloys are, for example, discussed by Y. Kakehashi, Progr. Theor. Phys. Suppl. **101**, 105 (1990).
[12] H. Akai, J. Phys. Condens. Matter **1**, 8045 (1989).
[13] H. Hasegawa and J. Kanamori, J. Phys. Soc. Jpn. **31**, 382 (1971).
[14] H. Hasegawa and J. Kanamori, J. Phys. Soc. Jpn. **33**, 1599 (1972).
[15] H. Hasegawa and J. Kanamori, J. Phys. Soc. Jpn. **33**, 1607 (1972).
[16] H. Akai, P. H. Dederichs, and J. Kanamori, J. Phys. (Paris) Colloq. **49**, C8-23 (1988).
[17] H. Akai and P. H. Dederichs, Phys. Rev. B **47**, 8739 (1993).
[18] Y. Kakehashi, J. Phys. Soc. Jpn. **50**, 2236 (1981).
[19] H. Akai, Physica B **86-88**, 539 (1977).
[20] G. M. Stocks, W. M. Temmermann, and B. L. Gyorffy, Phys. Rev. Lett. **41**, 339 (1978).
[21] H. Akai, J. Phys. Soc. Jpn. **50**, 70 (1982).
[22] H. Akai, J. Phys. Soc. Jpn. **51**, 468 (1982).
[23] H. Winter and G. M. Stocks, Phys. Rev. B **27**, 882 (1983).
[24] D. D. Johnson, D. M. Nicholson, F. J. Pinski, B. L. Gyorffy, and G. M. Stocks, Phys. Rev. Lett. **56**, 2088 (1986).
[25] D. D. Johnson and F. J. Pinski, J. Appl. Phys. **57**, 3018 (1985).
[26] A. R. Williams, R. Zeller, V. L. Moruzzi, and C. D. Gelattt, Jr., J. Appl. Phys. **52**, 2067 (1981).
[27] J. B. Staunton, Rep. Prog. Phys. **57**, 1289 (1994).
[28] D. D. Johnson, F. J. Pinski, and J. B. Staunton, J. Appl. Phys. **61**, 3715 (1987).
[29] O. Gunnarsson, O. Jepsen, and O. K. Anderson, Phys. Rev. B **27**, 7144 (1983).
[30] A. I. Liechtenstein, M. I. Katsnelson, V. P. Antropov, and V. A. Gubanov, J. Magn. Magn. Mater. **67**, 65 (1987).
[31] H. Köhler, J. Sticht, and J. Kübler, Physica B **172**, 79 (1991).
[32] M. Uhl, L. M. Sandratskii, and J. Kübler, Phys. Rev. B **50**, 291 (1994).
[33] Fluctuations in the data of total energies as function of lattice constant and magnetization have been smoothed down with the help of a Tschebyscheff polynomial (of 8×8 order) with a weighting factor $g(E) = \exp\{10^{-4}E^2(a, M)\}$, where $E(a, M)$ is taken in multiples of mRy and relative to the absolute energy minimum.
[34] V. L. Moruzzi, P. M. Marcus, K. Schwarz, and P. Mohn, Phys. Rev. B **34**, 1784 (1986).
[35] M. M. Abd-Almeguid and H. Micklitz, Physica B **161**, 17

(1989).
[36]M. Acet, H. Zähres, E. F. Wassermann, and W. Pepperhoff, Phys. Rev. B **49**, 6012 (1994).
[37]More properly: Previous conversion-electron Mössbauer spectroscopy and recent neutron-diffraction study of γ-Fe at high pressure in the temperature range from 5 to 110 K show that the fcc phase undergoes antiferromagnetic ordering at 67±2 K at ambient pressure: W. A. A. Macedo and W. Keune, Phys. Rev. Lett. **61**, 475 (1988); A. Onodera, Y. Tsunoda, N. Kunitomi, O. A. Pringle, R. M. Nicklow, and R. Moon, Phys. Rev. B **50**, 3532 (1994), respectively.
[38]G. L. Krasko and G. B. Olson, Phys. Rev. B **40**, 11 536 (1989).
[39]V. A. Makarov, I. M. Puzei, T. V. Sakharova, and O. V. Basargin, Sov. Phys. JETP **61**, 839 (1985).
[40]This might be the reason why the ground state of fcc Fe is a LM antiferromagnet: For the fcc crystal structure, the antibonding DOS peak lies just below E_F. The electrons (having mainly t_{2g} symmetry) show a tendency for antiferromagnetic correlations (being an easy way to fulfill Pauli's principle) which lead to a low-volume LM antiferromagnetic ground state. For the bcc crystal structure, the Fermi energy is more remote from this DOS peak allowing for ferromagnetic correlations which stabilize a high-volume HM ferromagnetic ground state; see also V. Heine, A. I. Liechtenstein, and O. N. Mryasov, Europhys. Lett. **12**, 545 (1990).
[41]M. F. Sykes, D. S. Gaunt, and Maureen Glen, J. Phys. A **9**, 1705 (1976).
[42]M. Podgorny, Acta Phys. Polon. A **78**, 941 (1990).
[43]M. Podgorny, Phys. Rev. B **43**, 11 300 (1991).
[44]R. J. Weiss, Proc. Phys. Soc. London **82**, 281 (1963).
[45]J. B. Müller and J. Hesse, Z. Phys. B **54**, 35 (1983); **54**, 43 (1983).
[46]A. R. Williams, V. L. Moruzzi, C. D. Gelatt, Jr., and J. Kübler, J. Magn. Magn. Mater. **31-33**, 88 (1983).
[47]V. L. Moruzzi, Phys. Rev. B **41**, 6939 (1990).
[48]V. L. Moruzzi, Solid State Commun. **83**, 739 (1992).
[49]V. L. Moruzzi, in *Isomes '89, Proceedings of the International Symposium on Magnetoelasticty and Electronic Structure of Transition Metals, Alloys, and Films* (Ref. 1), p. 99.
[50]E. G. Moroni and T. Jarlborg, J. Magn. Magn. Mater. **104-107**, 711 (1992).
[51]P. Entel and M. Schröter, J. Phys. (Paris) Colloq. **49**, C8-293 (1988).
[52]P. Entel and M. Schröter, Physica B **161**, 121 (1989).
[53]D. Wagner, J. Phys. Condens. Matter **1**, 4635 (1989).
[54]M. Schröter, P. Entel, and S. G. Mishra, J. Magn. Magn. Mater. **87**, 163 (1990).
[55]P. Mohn, K. Schwarz, and D. Wagner, Phys. Rev. B **43**, 3318 (1991).
[56]M. Schröter, Ph.D. thesis, University of Duisburg, 1992.
[57]B. L. Gyorffy, J. Kollar, A. J. Pindor, G. M. Stocks, J. Staunton, and H. Winter, in *The Electronic Structure of Complex Systems*, Vol. 113 of *NATO ASI Series B: Physics*, edited by P. Phariseau and W. M. Temmerman (Plenum, New York, 1982), p. 593.
[58]M. B. Taylor, B. L. Gyorffy, and C. J. Walden, J. Phys. Condens. Matter **3**, 1575 (1991).
[59]E. Hoffmann, H. Herper, P. Entel, S. G. Mishra, P. Mohn, and K. Schwarz, Phys. Rev. B **47**, 5589 (1993).
[60]H. Hasegawa, J. Phys. Soc. Jpn. **49**, 963 (1980).
[61]J. A. Morkowski and P. Wosicki, J. Magn. Magn. Mater. **71**, 285 (1988).
[62]For state of the art of spin-fluctuation theories, see T. Moriya, *Spin Fluctuations in Itinerant Electron Magnetism*, (Springer, Berlin, 1985); *Metallic Magnetism*, edited by H. Capellmann (Springer, Berlin, 1987).
[63]T. Moriya, Solid State Commun. **26**, 483 (1978).
[64]P. Mohn and G. Hilscher, Phys. Rev. B **40**, 9126 (1989).
[65]W. Bendick, H. H. Ettwig, and W. Pepperhoff, J. Phys. F **8**, 2525 (1978).
[66]N. Schubert, Ph.D. thesis, University of Duisburg, 1993.
[67]A. V. Deryabin, V. I. Rimlyand, and A. P. Larionov, Sov. Phys. Solid State **25**, 1109 (1983).
[68]B. Rellinghaus, J. Kästner, Th. Schneider, E. F. Wassermann, and P. Mohn, Phys. Rev. B **51**, 2983 (1995).
[69]The Landau coefficients in Table II are of optimum choice and reproduce well the zero-temperature KKR-CPA binding surfaces. Gradient terms $g_m = 1.4$, $g_\omega = 1.4$ and cutoff parameters for momentum integration $q_m = 8$ and $q_\omega = 8$ at finite temperatures are a compromise. Large cutoff parameters are needed to suppress first-order phase transitions lowering at the same time the Curie temperature. The equal-time correlation function in Fig. 13 has been obtained by changing c in Table II to $c = 0.4000$ and by using $q_m = 3.67$, $q_\omega = 7.2$. This yields $T_c = 548$ K.
[70]O. Yamada, F. Ono, H. Nakai, H. Maruyama, F. Arae, and K. Ohta, Solid State Commun. **42**, 473 (1982).
[71]K Tajima, P. Böni, G. Shirane, Y. Ishikawa, and M. Kohgi, Phys. Rev. B **35**, 274 (1987).
[72]J. Wicksted, P. Böni, and G. Shirane, Phys. Rev. B **30**, 3655 (1984).
[73]M. Kohgi, Y. Ishikawa, and N. Wakabayashi, Solid State Commun. **18**, 509 (1976).
[74]G. Shirane, P. Böni, and J. Wicksted, Phys. Rev. B **33**, 1881 (1986).
[75]O. Steinsvoll, C. F. Majkrzak, G. Shirane, and J. Wicksted, Phys. Rev. B **30**, 2377 (1984).
[76]H. Hasegawa, J. Phys. F **13**, 2655 (1983).
[77]H. Hasegawa, J. Phys. F **14**, 1235 (1984).
[78]P. J. Brown, H. Capellmann, J. Déportes, D. Givord, and K. R. A. Ziebeck, J. Magn. Magn. Mater. **30**, 243 (1982).
[79]S. Hirooka and M. Shimizu, J. Phys. F **18**, L127 (1988).
[80]M. Weiner, E. Wimmer, and A. J. Freeman, Phys. Rev. B **26**, 4571 (1982).
[81]M Shiga, K. Makita, K. Uematsu, Y. Muraoka, and Y. Nakamura, J. Phys. Condens. Matter **2**, 1239 (1990).
[82]G. A. Alers, J. R. Neighbours, and H. Sato, J. Phys. Chem. Solids **13**, 40 (1960).
[83]G. Hausch, Phys. Status Solidi A **15**, 501 (1973).
[84]P. Hong and G. B. Olson, J. Magn. Magn. Mater. **129**, 191 (1994).
[85]J. Crangle and G. C. Hallam, Proc. R. Soc. (London) **32**, 119 (1963).
[86]S. Chikazumi, T. Mizoguchi, N, Yamaguchi, and P. Beckwith, J. Appl. Phys. **39**, 939 (1968).
[87]M. Hansen, *Constitution of Binary Alloys* (McGraw-Hill, New York, 1958).
[88]M. Acet, T. Schneider, and E. F. Wassermann, J. Phys. (France) IV **5**, C2-105 (1995).
[89]T. Miyazaki, Y. Ando, and M. Takahashi, J. Appl. Phys. **57**, 3456 (1985).
[90]I. A. Abrikosov, O. Eriksson, P. Söderlind, H. L. Skriver, and B. Johansson, Phys. Rev. B **51**, 1058 (1995).
[91]E. G. Moroni, P. Lerch, and T. Jarlborg, Phys. Rev. B **49**, 11 979 (1994); E. G. Moroni and T. Jarlborg, J. Appl. Phys. **75**, 6571 (1994).